CHAPTER 7

HEALTH MONITORING ON THE TEST FRAME

7.1 Introduction

In Chapters 4 and 5, neural network-based system identification methods and a two-stage damage assessment approach were proposed and examined by either numerical examples or laboratory measurements. The examined results have preliminarily shown their capabilities of dealing with the associated problems. By conducting a series of shaking table tests for the health monitoring study, the proposed methods and approach are further investigated by the experimental measurements.

In implementing the health monitoring of the test structure, three strategies are carried out. By using the first strategy, the acceleration measurements of each simulated deterioration case are first analyzed using the ANNSI model to generate the modal frequencies and displacement modal shapes of the test structure. The structural condition of the specimen can then be diagnosed based on the identified modal data change. In the second strategy, the health monitoring of the test structure is basing on the changes in strain mode shape information. The strain mode shapes are extracted from the FBG sensors and RSGs measurements by also using the ANNSI model. Moreover, the global and decentralized monitoring networks are adopted for the purpose of health monitoring using the structural acceleration and strain measurements

in the third strategy. The three strategies are sequentially introduced in the subsequent sections. Notably, according to the nature of the damage detection procedure in the strategy, the first strategy is model-based; while the second and third strategies are non-model-based. Moreover, though three different strategies for structural health monitoring are utilized, they should produce similar diagnostic results.

7.2 Modal Analysis Using The ANNSI Model

Based on the empirical and trail-and-error methods as well as the preliminarily analysis on the Fourier spectra of the experimental measurements, the appropriate architecture of the modal analysis network (MAN) in ANNSI model is determined. The acceleration measurements are first analyzed to obtain the corresponding modal parameters. Subsequently, the strain measurements from the FBG sensors and RSGs are also analyzed to generate the strain mode shapes information. Those modal data will be further applied to monitor and assess the structural conditions.

7.2.1 Modal Data of the Specimen Extracted from the Acceleration Measurements

The acceleration measurements from the intact structure (i.e. AAA_acc, in Table 6.10) are first analyzed using the ANNSI model to obtain the baseline information. Figure 7.1 presents the response time-histories of the AAA_acc measurement. It is seen that, the larger responses happened to the time between 4.5 and 15 seconds. Therefore, the measurements between 5 and 12.5 seconds (i.e. 1500 records with 200Hz sampling rate) are used throughout this chapter to train the neural networks. Figure 7.2 shows the

excellent correspondence between the measured responses and the computed responses from the trained MAN.

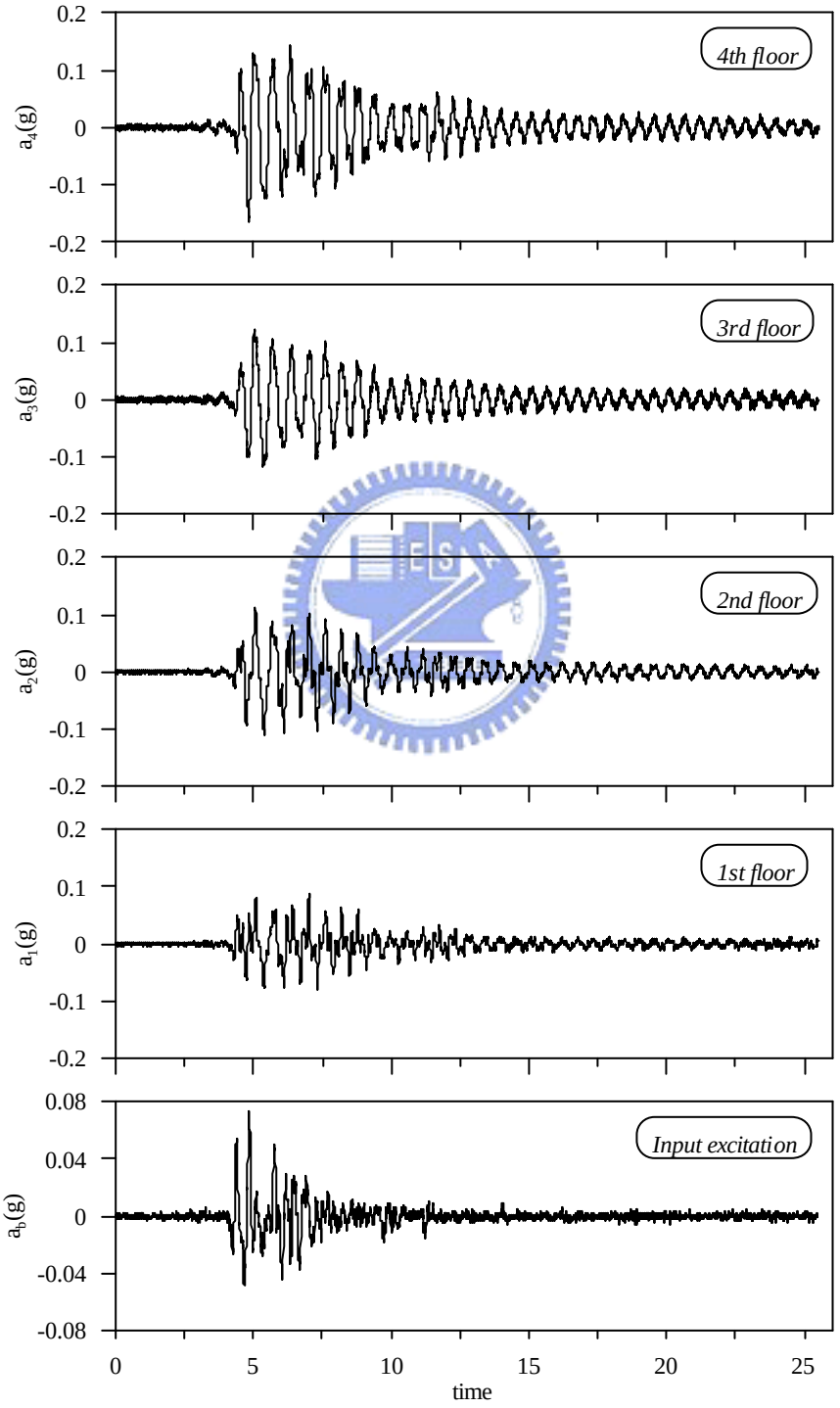

Figure 7.1 Response histories of the AAA_acc measurement

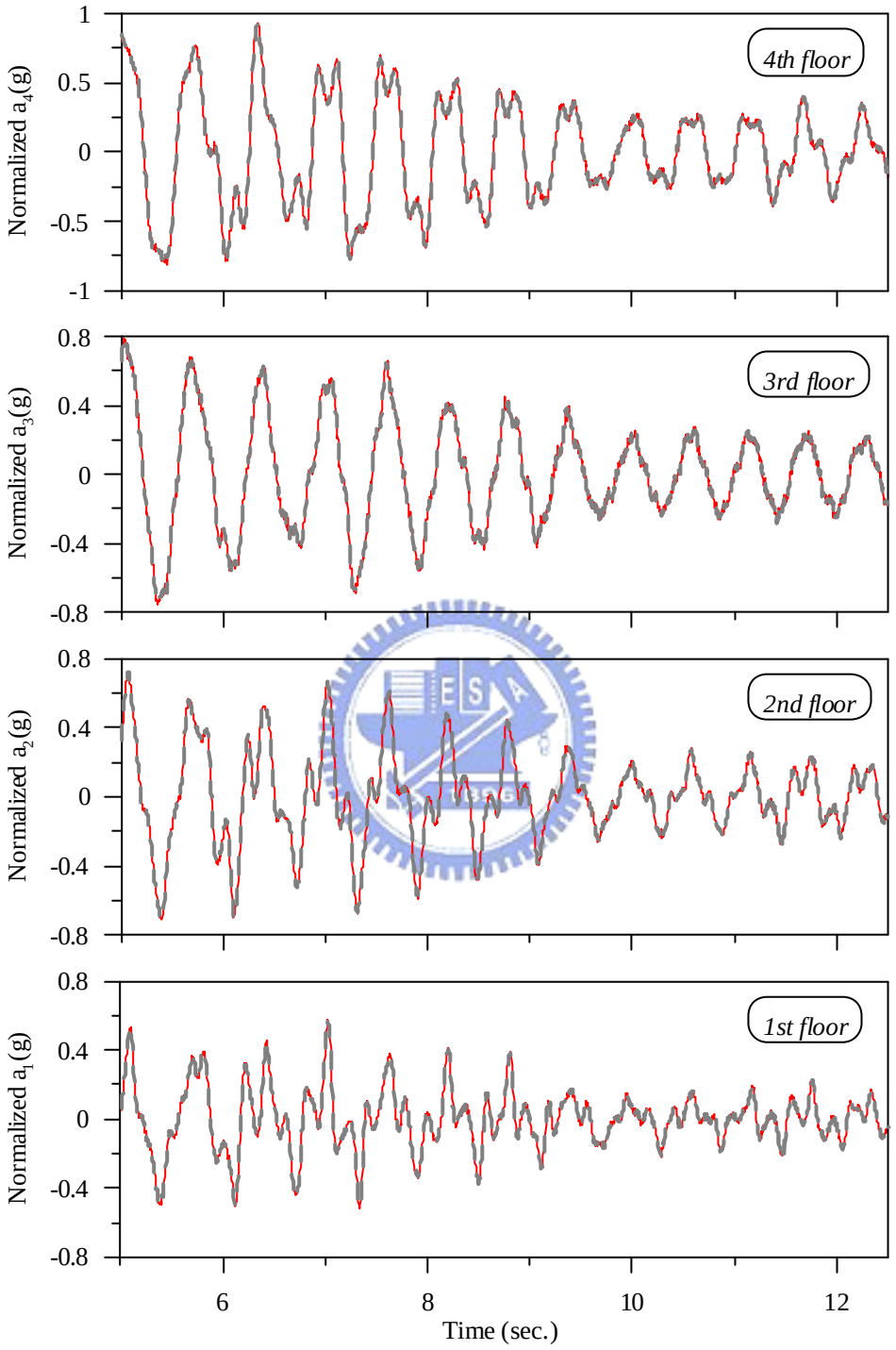

Figure 7.2 Comparison between the measured (solid line) and computed (dash line) responses for the AAA_acc measurement

After the MAN was trained by the AAA_acc measurement, the modal parameters of the intact structure can be estimated basing on the connective weights of the trained MAN. The identified baseline modal data extracted from the acceleration measurements are shown in Table 7.1.

Table 7.1 Modal parameters of the test structure in healthy condition (*AAA*)

Mode		**1**	**2**	**3**	**4**
Frequency (Hz)		1.69	5.04	8.14	10.22
Damping ratio (%)		3.32	1.38	1.40	2.01
Mode shape	**A4**	1.000	1.000	0.427	0.288
	A3	0.846	-0.130	-0.729	-0.729
	A2	0.628	-0.914	-0.137	1.000
	A1	0.336	-0.830	1.000	-0.705

Basing on the aforementioned MAN structure, each of the rest acceleration measurements obtained from the shaking table tests on the simulated deteriorated structures is trained by a MAN and then extracted the corresponding modal parameters from it. Tables 7.2 to 7.25 show the modal parameters for each simulated deterioration case listed in Table 6.9. Note that, the *MAC* values in those tables were computed with respect to the mode shapes of the intact structure.

For comparison, the natural frequencies and damping ratios in all deterioration cases are schematically depicted in Figures 7.3 and 7.4, respectively. In addition, Figures 7.5 and 7.6 present the relative changes in natural frequencies and damping ratios with respect to the baseline values. In Figure 7.5, a value of 3% (two dash lines in the figure) is adopted as a criterion for representing the slight (or detectable) change.

The reason for selecting this value is that it would be necessary for a natural frequency to change by about 5% for damage to be detected with confidence [14]; hence 3% is adopted for conservation.

According to the tables and figures, some discussions are addressed below.

(1) As discussed in section 6.6.1, the effect of replacing the smaller SCs is much lesser than that of removing the SCs; therefore, the modal parameters changed more when the SCs were removed from the test structure. For example, according to Figure 7.5, the relative changes in the 1st modal frequency of the low-level deterioration scenarios, such as *Dcase_BAA*, *Dcase_ABA*, and *Dcase_AAB*, are within the criterion (i.e. the relative changes in frequencies are lower than 3%); while the relative changes in the 1st modal frequency of the high-level deterioration scenarios, such as *Dcase_NAA*, *Dcase_ANA*, and *Dcase_AAN*, are beyond the criterion.

(2) According to Tables 7.1, 7.2, 7.4, and 7.6, the 1st modal frequencies of the low-level deterioration scenarios are very close to each other. In addition, the 1st and 2nd modal frequencies of *Dcase_ABA* are slightly higher than the baseline values. As known, the loss of mass and enhancement of stiffness increase the natural frequencies. Though the stiffness provided by the SC-A is more than by the SC-B, the SC-A is heavier than the SC-B. Accordingly, the reason for the above circumstance may be that the effectiveness of the stiffness to the 1st and 2nd modes of *Dcase_ABA* is lower than that of the mass.

(3) According to Figure 7.5, the amount of variations in each modal frequency varied with the deteriorated site. Take the single-site deterioration cases for

examples, the changes in every modal frequencies exceed 3% and the 1st modal frequency changed the most in *Dcase_NAA* (which belongs to *Dclass_k*$_1$); for *Dcase_ANA* (which belongs to *Dclass_k*$_2$), the changes in the 1st, 3rd, and 4th modal frequencies exceed 3% and with similar quantity, while insignificant change happens to the 2nd modal frequency; for *Dcase_AAN* (which belongs to *Dclass_k*$_3$), the changes in every modal frequencies exceed 3% and the 4th modal frequency changed the most.

(4) Since the structures of the cases of *Dclass_k*$_1$&*k*$_2$ are deteriorated at the 1st and 2nd stories, they should exhibit the properties of *Dclass_k*$_1$ and *Dclass_k*$_2$ mentioned in last discussion. In *Dcase_NBA*, the structure was deteriorated at the 1st and 2nd stories, and the deterioration extent at the 1st story is higher than at the 2nd story. Therefore, the amounts of changes in modal frequencies for all modes exceed 3%. Moreover, the structure deteriorated more seriously at the 2nd story than at the 1st story in *Dcase_BNA*, which causes changes in modal frequencies for all modes except for the 2nd mode exceed 3%. Similar situations also happen to the cases of *Dclass_k*$_1$&*k*$_3$ and *Dclass_k*$_2$&*k*$_3$.

(5) Though certain measurements produced the same identified results on the 1st modal frequency, such as *Dcase_NAA*, *Dcase_BNA*, *Dcase_NAB*, and *Dcase_NBB*, the rest modal frequencies of these cases are different from each others because they belong to different deterioration classes. Therefore, it is quite difficult to detect structural deterioration basing only on one modal frequency in the modal-based deterioration detection methods.

Table 7.2 Modal parameters of *Dcase_BAA*

Mode		**1**	**2**	**3**	**4**
Frequency (Hz)		1.68	4.94	7.89	10.17
Damping ratio (%)		2.54	1.23	0.54	3.04
Mode shape	**A4**	1.000	1.000	0.557	0.254
	A3	0.844	-0.100	-0.893	-0.775
	A2	0.629	-0.935	-0.206	1.000
	A1	0.340	-0.887	1.000	-0.672
MAC		1.000	0.999	0.989	0.998

Table 7.3 Modal parameters of *Dcase_NAA*

Mode		**1**	**2**	**3**	**4**
Frequency (Hz)		1.60	4.78	7.77	9.88
Damping ratio (%)		1.80	0.28	0.49	2.53
Mode shape	**A4**	1.000	1.000	0.582	0.317
	A3	0.857	-0.035	-0.870	-0.809
	A2	0.649	-0.879	-0.303	1.000
	A1	0.370	-0.932	1.000	-0.618
MAC		1.000	0.992	0.979	0.993

Table 7.4 Modal parameters of *Dcase_ABA*

Mode		**1**	**2**	**3**	**4**
Frequency (Hz)		1.70	5.09	7.93	10.15
Damping ratio (%)		2.11	0.50	1.27	2.68
Mode shape	**A4**	1.000	1.000	0.449	0.249
	A3	0.843	-0.149	-0.769	-0.871
	A2	0.648	-0.835	-0.197	1.000
	A1	0.344	-0.786	1.000	-0.757
MAC		1.000	0.998	0.998	0.993

Table 7.5 Modal parameters of *Dcase_ANA*

Mode		**1**	**2**	**3**	**4**
Frequency (Hz)		1.63	5.02	7.84	9.85
Damping ratio (%)		1.78	0.69	4.64	4.26
Mode shape	**A4**	1.000	1.000	0.415	0.388
	A3	0.856	-0.121	-0.614	-0.923
	A2	0.671	-0.823	-0.214	1.000
	A1	0.326	-0.829	1.000	-0.640
MAC		0.999	0.998	0.989	0.982

Table 7.6 Modal parameters of *Dcase_AAB*

Mode		**1**	**2**	**3**	**4**
Frequency (Hz)		1.68	5.03	7.97	10.10
Damping ratio (%)		2.80	0.33	2.23	1.32
Mode shape	**A4**	1.000	1.000	0.609	0.277
	A3	0.852	-0.119	-0.951	-0.836
	A2	0.638	-0.885	-0.176	1.000
	A1	0.337	-0.827	1.000	-0.709
MAC		1.000	1.000	0.981	0.996

Table 7.7 Modal parameters of *Dcase_AAN*

Mode		**1**	**2**	**3**	**4**
Frequency (Hz)		1.63	4.84	7.70	9.65
Damping ratio (%)		2.92	0.28	1.22	1.64
Mode shape	**A4**	1.000	0.955	0.692	0.284
	A3	0.852	-0.042	-1.000	-0.723
	A2	0.602	-1.000	-0.134	1.000
	A1	0.317	-0.909	0.928	-0.866
MAC		1.000	0.993	0.955	0.991

Table 7.8 Modal parameters of *Dcase_BBA*

Mode		**1**	**2**	**3**	**4**
Frequency (Hz)		1.62	4.89	7.72	10.08
Damping ratio (%)		2.50	1.64	0.53	2.52
Mode shape	**A4**	1.000	1.000	0.558	0.351
	A3	0.855	-0.075	-0.829	-0.807
	A2	0.649	-0.855	-0.252	1.000
	A1	0.354	-0.832	1.000	-0.565
MAC		1.000	0.998	0.988	0.986

Table 7.9 Modal parameters of *Dcase_BNA*

Mode		**1**	**2**	**3**	**4**
Frequency (Hz)		1.60	4.91	7.49	9.68
Damping ratio (%)		1.75	1.03	0.56	1.32
Mode shape	**A4**	1.000	1.000	0.532	0.361
	A3	0.859	-0.086	-0.755	-0.954
	A2	0.654	-0.934	-0.294	1.000
	A1	0.319	-0.855	1.000	-0.547
MAC		1.000	0.999	0.985	0.967

Table 7.10 Modal parameters of *Dcase_NBA*

Mode		**1**	**2**	**3**	**4**
Frequency (Hz)		1.58	4.76	7.59	9.49
Damping ratio (%)		1.47	0.50	0.65	3.27
Mode shape	**A4**	1.000	1.000	0.564	0.312
	A3	0.863	-0.025	-0.807	-0.826
	A2	0.657	-0.883	-0.336	1.000
	A1	0.363	-0.957	1.000	-0.685
MAC		1.000	0.990	0.977	0.996

Table 7.11 Modal parameters of *Dcase_NNA*

Mode		**1**	**2**	**3**	**4**
Frequency (Hz)		1.55	4.72	7.38	9.62
Damping ratio (%)		0.72	0.66	0.34	0.62
Mode shape	**A4**	1.000	1.000	0.520	0.352
	A3	0.868	-0.014	-0.682	-0.982
	A2	0.668	-0.918	-0.382	1.000
	A1	0.349	-0.934	1.000	-0.546
MAC		1.000	0.992	0.964	0.962

Table 7.12 Modal parameters of *Dcase_BAB*

Mode		**1**	**2**	**3**	**4**
Frequency (Hz)		1.63	4.90	7.81	10.04
Damping ratio (%)		2.31	0.25	0.88	1.08
Mode shape	**A4**	1.000	1.000	0.610	0.294
	A3	0.855	-0.063	-0.920	-0.808
	A2	0.653	-0.844	-0.205	1.000
	A1	0.355	-0.824	1.000	-0.671
MAC		1.000	0.997	0.983	0.997

Table 7.13 Modal parameters of *Dcase_BAN*

Mode		**1**	**2**	**3**	**4**
Frequency (Hz)		1.59	4.72	7.74	9.70
Damping ratio (%)		2.58	0.11	0.31	2.17
Mode shape	**A4**	1.000	0.985	0.675	0.246
	A3	0.859	-0.014	-1.000	-0.948
	A2	0.619	-1.000	-0.094	1.000
	A1	0.335	-0.946	0.863	-0.847
MAC		1.000	0.991	0.941	0.985

Table 7.14 Modal parameters of *Dcase_NAB*

Mode		**1**	**2**	**3**	**4**
Frequency (Hz)		1.60	4.84	7.71	9.99
Damping ratio (%)		1.49	0.21	0.79	0.62
Mode shape	**A4**	1.000	1.000	0.632	0.289
	A3	0.860	-0.044	-0.942	-0.808
	A2	0.667	-0.835	-0.273	1.000
	A1	0.371	-0.889	1.000	-0.603
MAC		0.999	0.993	0.975	0.992

Table 7.15 Modal parameters of *Dcase_NAN*

Mode		**1**	**2**	**3**	**4**
Frequency (Hz)		1.56	4.63	7.67	9.65
Damping ratio (%)		1.42	0.04	0.20	2.33
Mode shape	**A4**	1.000	0.978	0.698	0.282
	A3	0.862	0.026	-1.000	-0.703
	A2	0.627	-0.959	-0.163	1.000
	A1	0.348	-1.000	0.803	-0.771
MAC		1.000	0.983	0.923	0.998

Table 7.16 Modal parameters of *Dcase_ABB*

Mode		**1**	**2**	**3**	**4**
Frequency (Hz)		1.68	5.02	7.86	10.07
Damping ratio (%)		2.31	0.31	1.67	1.12
Mode shape	**A4**	1.000	1.000	0.559	0.262
	A3	0.848	-0.118	-0.871	-0.832
	A2	0.637	-0.888	-0.171	1.000
	A1	0.337	-0.815	1.000	-0.680
MAC		1.000	1.000	0.991	0.995

Table 7.17 Modal parameters of *Dcase_ABN*

Mode		**1**	**2**	**3**	**4**
Frequency (Hz)		1.64	4.84	7.77	9.58
Damping ratio (%)		2.08	0.16	0.24	1.76
Mode shape	**A4**	1.000	0.953	0.660	0.332
	A3	0.853	-0.049	-1.000	-0.760
	A2	0.598	-1.000	-0.068	1.000
	A1	0.313	-0.876	0.890	-0.780
MAC		0.999	0.994	0.952	0.998

Table 7.18 Modal parameters of *Dcase_ANB*

Mode		**1**	**2**	**3**	**4**
Frequency (Hz)		1.61	4.90	7.68	9.76
Damping ratio (%)		1.59	0.21	1.65	0.70
Mode shape	**A4**	1.000	1.000	0.483	0.277
	A3	0.859	-0.075	-0.702	-0.826
	A2	0.660	-0.858	-0.211	1.000
	A1	0.321	-0.867	1.000	-0.492
MAC		1.000	0.997	0.995	0.974

Table 7.19 Modal parameters of *Dcase_ANN*

Mode		**1**	**2**	**3**	**4**
Frequency (Hz)		1.57	4.74	7.59	9.26
Damping ratio (%)		1.51	0.31	0.28	0.43
Mode shape	**A4**	1.000	0.987	0.626	0.411
	A3	0.861	-0.027	-0.853	-0.929
	A2	0.623	-1.000	-0.182	1.000
	A1	0.303	-0.920	1.000	-0.670
MAC		0.999	0.993	0.985	0.982

Table 7.20 Modal parameters of *Dcase_BBB*

Mode		**1**	**2**	**3**	**4**
Frequency (Hz)		1.62	4.88	7.79	9.90
Damping ratio (%)		2.24	0.36	0.76	1.40
Mode shape	**A4**	1.000	1.000	0.559	0.304
	A3	0.856	-0.061	-0.895	-0.919
	A2	0.653	-0.845	-0.198	1.000
	A1	0.355	-0.840	1.000	-0.642
MAC		1.000	0.997	0.989	0.985

Table 7.21 Modal parameters of *Dcase_BBN*

Mode		**1**	**2**	**3**	**4**
Frequency (Hz)		1.58	4.72	7.74	9.60
Damping ratio (%)		2.05	0.24	0.08	2.96
Mode shape	**A4**	1.000	0.990	0.669	0.309
	A3	0.860	-0.025	-1.000	-0.713
	A2	0.620	-1.000	-0.098	1.000
	A1	0.337	-0.929	0.934	-0.795
MAC		1.000	0.993	0.958	0.997

Table 7.22 Modal parameters of *Dcase_NBB*

Mode		**1**	**2**	**3**	**4**
Frequency (Hz)		1.60	4.82	7.63	9.92
Damping ratio (%)		0.81	0.29	0.50	0.57
Mode shape	**A4**	1.000	1.000	0.608	0.342
	A3	0.859	-0.044	-0.893	-0.796
	A2	0.662	-0.837	-0.301	1.000
	A1	0.373	-0.874	1.000	-0.578
MAC		0.999	0.994	0.977	0.989

Table 7.23 Modal parameters of *Dcase_BNN*

Mode		**1**	**2**	**3**	**4**
Frequency (Hz)		1.54	4.65	7.54	9.25
Damping ratio (%)		0.98	0.08	0.28	0.41
Mode shape	**A4**	1.000	1.000	0.612	0.391
	A3	0.867	0.019	-0.866	-0.934
	A2	0.636	-0.985	-0.195	1.000
	A1	0.324	-0.970	1.000	-0.671
MAC		1.000	0.987	0.986	0.983

Table 7.24 Modal parameters of *Dcase_NNB*

Mode		**1**	**2**	**3**	**4**
Frequency (Hz)		1.56	4.81	7.36	9.81
Damping ratio (%)		0.38	0.10	0.12	1.86
Mode shape	**A4**	1.000	1.000	0.568	0.370
	A3	0.866	-0.042	-0.745	-0.985
	A2	0.678	-0.850	-0.380	1.000
	A1	0.355	-0.890	1.000	-0.473
MAC		0.999	0.994	0.966	0.946

Table 7.25 Modal parameters of *Dcase_NNN*

Mode		**1**	**2**	**3**	**4**
Frequency (Hz)		1.52	4.64	7.33	9.23
Damping ratio (%)		0.23	0.10	0.17	0.50
Mode shape	**A4**	1.000	1.000	0.656	0.368
	A3	0.870	0.025	-0.845	-0.924
	A2	0.643	-0.980	-0.360	1.000
	A1	0.334	-0.970	1.000	-0.640
MAC		1.000	0.987	0.964	0.983

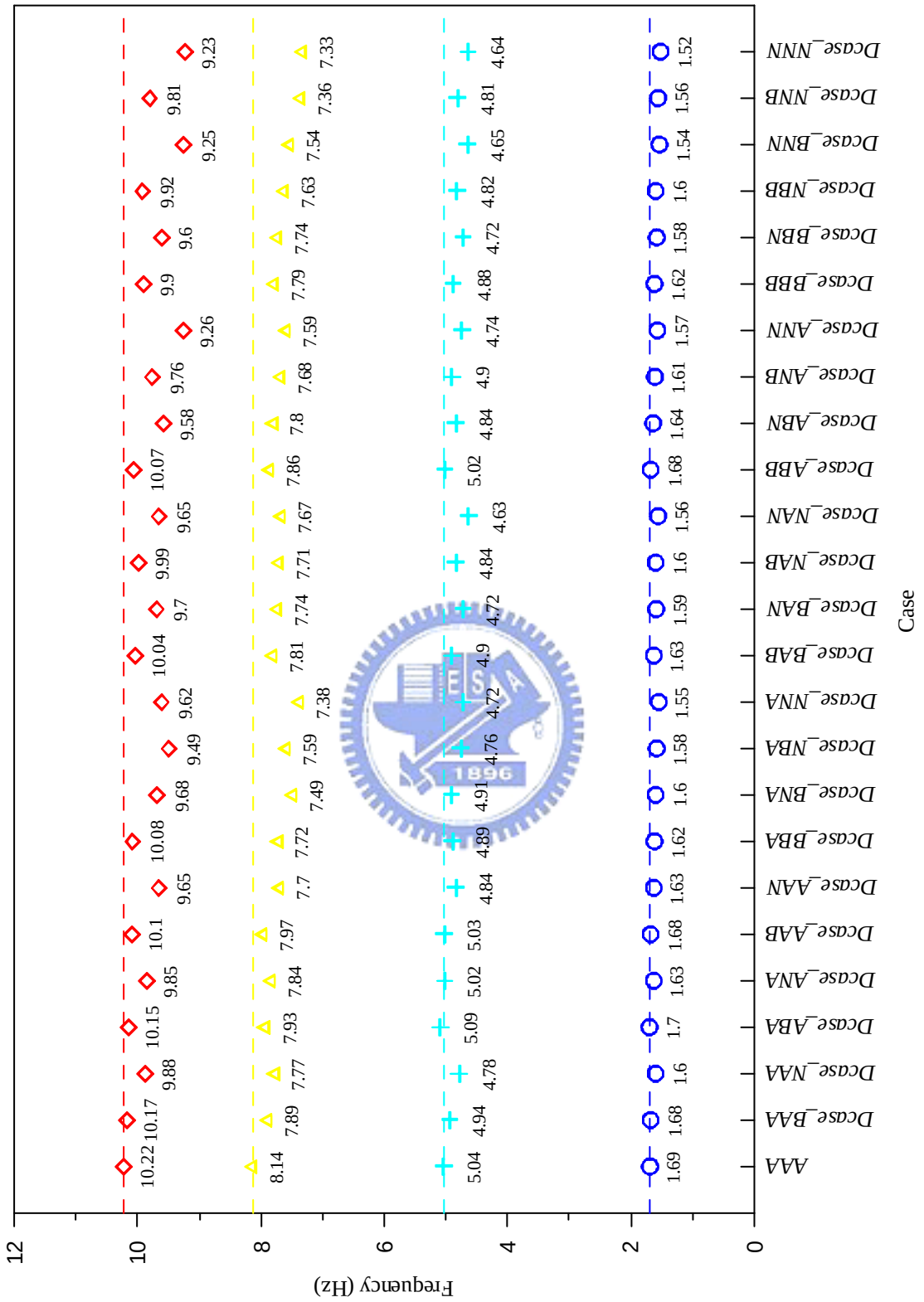

Figure 7.3 Variations of natural frequency under different deteriorated cases

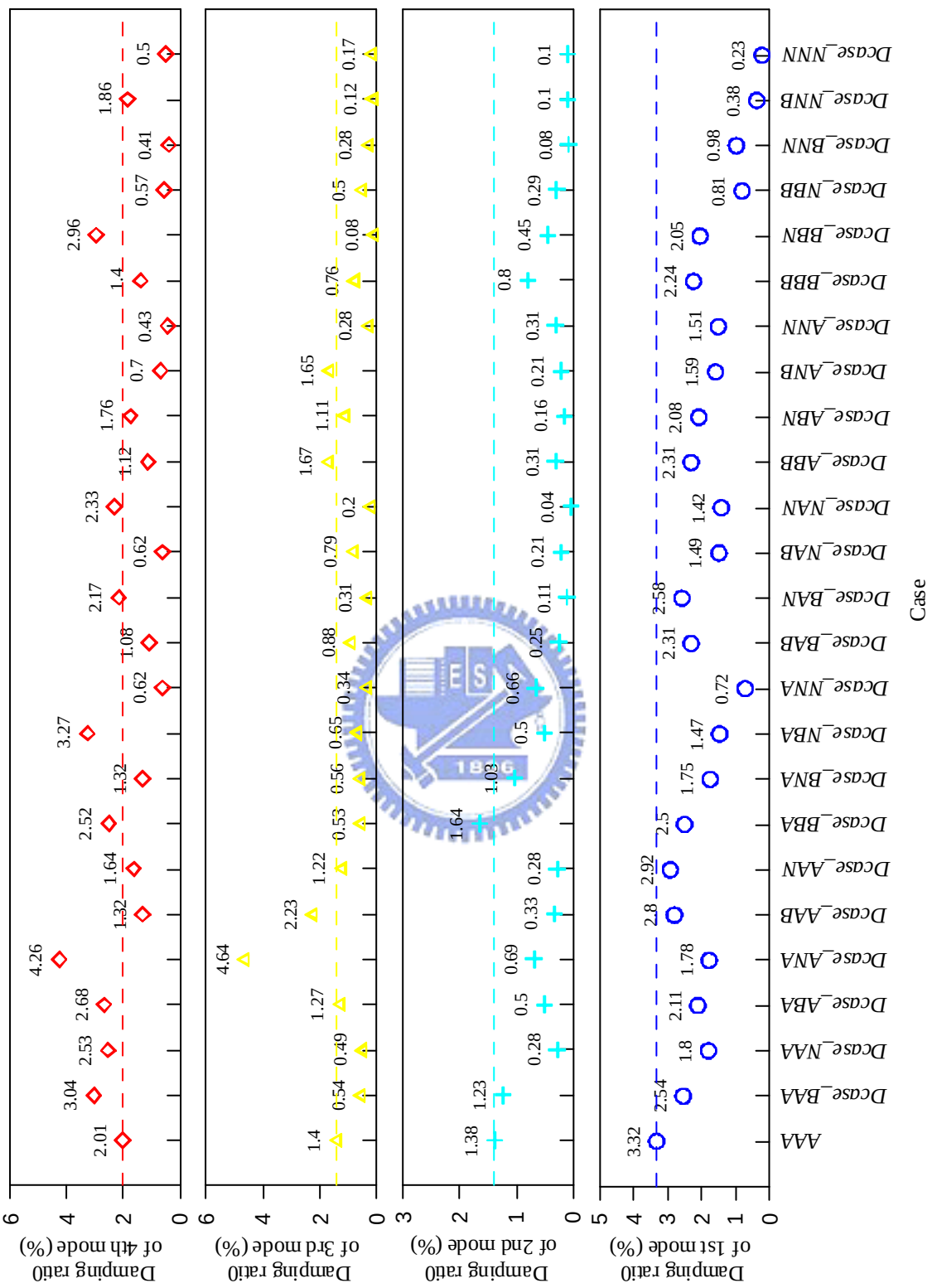

Figure 7.4 Variations of damping ratio under different deteriorated cases

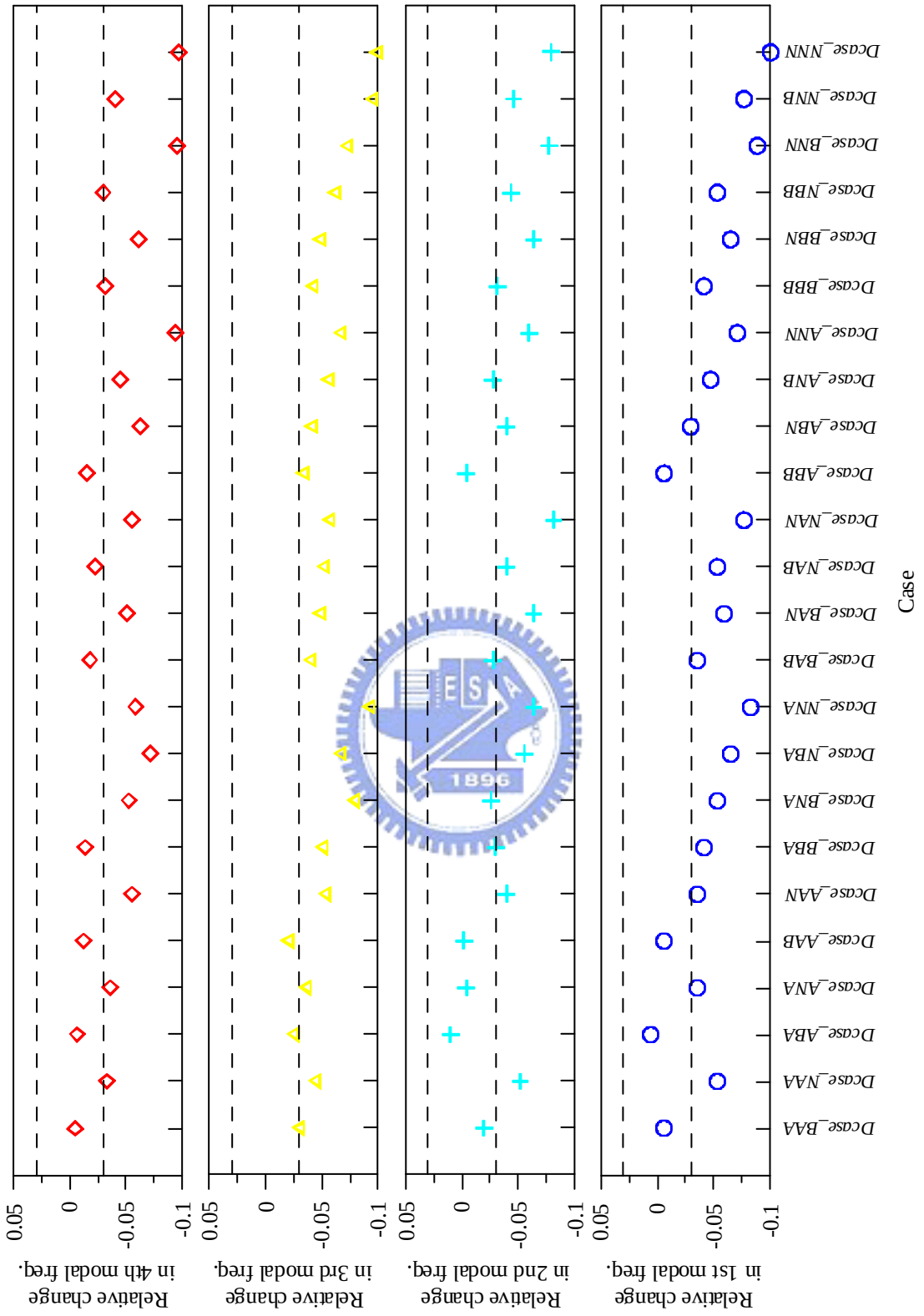

Figure 7.5 Relative changes in natural frequencies

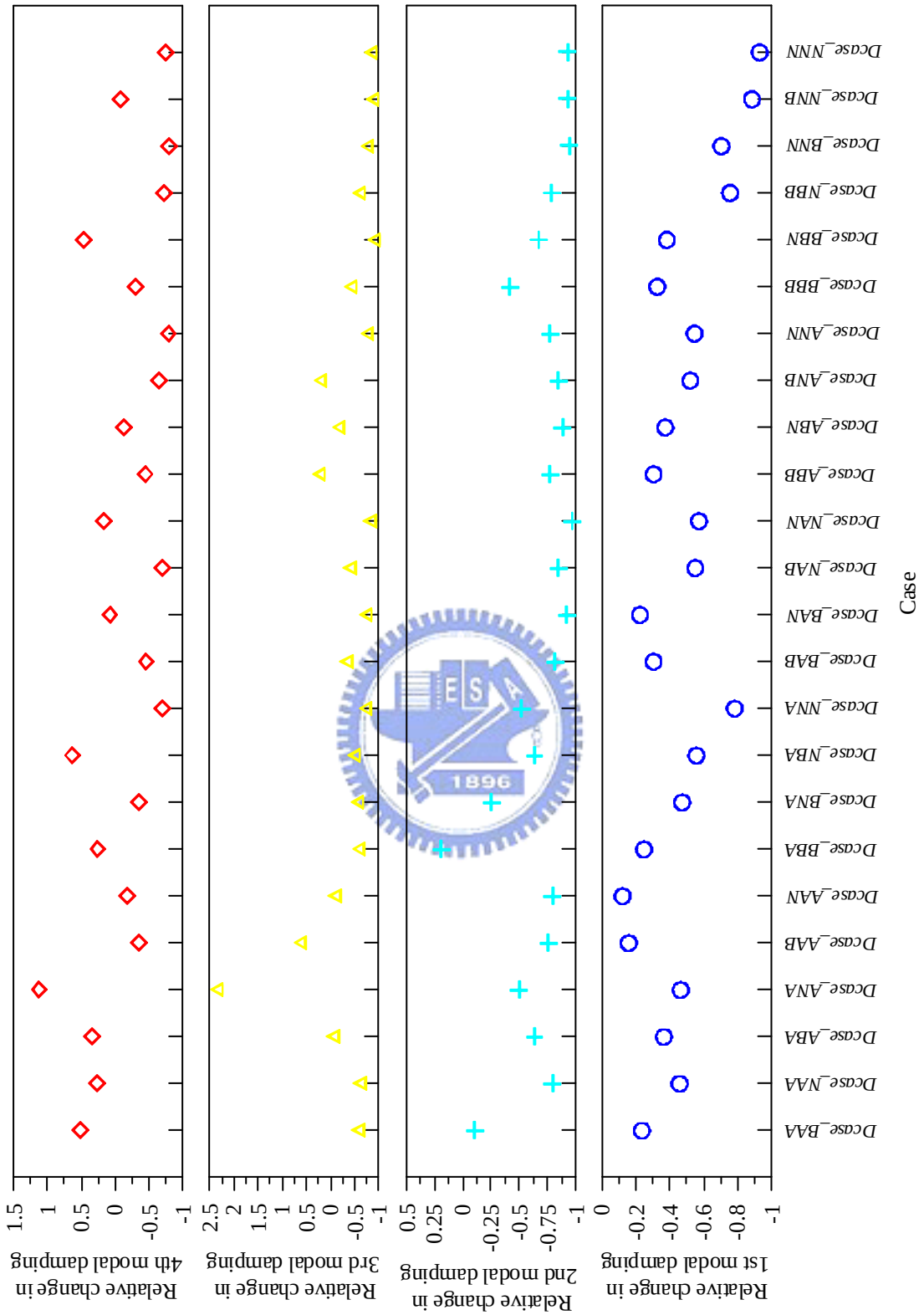

Figure 7.6 Relative changes in damping ratios

7.2.2 Modal Data of the Specimen Extracted from the RSGs Measurements

Since the structural strains can reflect local changes in a structure, the strain mode shapes (SMSs) would be a sensitive indicator for identifying the location of the structural damage. In the experiments of this work, two sets of strain data from the RSGs and the FBG sensors were recorded. The ANNSI model is also applied to the observed strain measurements to obtain the SMSs of the specimen.

The strain measurements from the RSGs were first analyzed. The identified modal parameters are listed in Tables 7.26 to 7.50. According to the experiences during modal analysis and these tables, some observations are discussed below.

(1) The order needed for the 1st and 2nd modes to be identified is lower than that for the 3rd and 4th modes. This may caused by the noise that contaminated in the RSGs measurements.

(2) Compare with the modes been identified from the acceleration measurements, only the first three modes can be identified from the RSGs measurements for most cases except for *Dcase_NNA*, *Dcase_BAB*, and *Dcase_ANN*.

(3) The 1st and 2nd modal frequencies been identified from acceleration and RSGs measurements are almost identical. Though the 3rd modal frequency been identified from the RSGs measurements is slight differ from that from the acceleration measurements, the maximum discrepancy between them is lesser than 1.2% (*Dcase_AAN*).

(4) The modal damping been identified from the RSGs measurements is close to the one from the acceleration measurements.

Table 7.26 Modal parameters of *AAA* using RSGs measurements

Mode		**1**	**2**	**3**	**4**
Frequency (Hz)		1.69	5.04	8.15	/
Damping ratio (%)		3.72	1.87	2.53	/
SMS	***RSG4***	0.524	1.000	1.000	/
	RSG3	0.731	0.594	-0.478	/
	RSG2	0.914	-0.110	-0.842	/
	RSG1	1.000	-0.740	0.805	/

Table 7.27 Modal parameters of *Dcase_BAA* using RSGs measurements

Mode		**1**	**2**	**3**	**4**
Frequency (Hz)		1.68	4.96	7.97	/
Damping ratio (%)		2.77	1.83	2.57	/
SMS	***RSG4***	0.521	1.000	1.000	/
	RSG3	0.733	0.633	-0.328	/
	RSG2	0.922	-0.130	-0.580	/
	RSG1	1.000	-0.724	0.629	/

Table 7.28 Modal parameters of *Dcase_NAA* using RSGs measurements

Mode		**1**	**2**	**3**	**4**
Frequency (Hz)		1.60	4.79	7.76	/
Damping ratio (%)		1.91	0.40	1.07	/
SMS	***RSG4***	0.431	1.000	1.000	/
	RSG3	0.651	0.771	-0.446	/
	RSG2	0.793	0.033	-0.828	/
	RSG1	1.000	-0.881	0.647	/

Table 7.29 Modal parameters of *Dcase_ABA* using RSGs measurements

Mode		**1**	**2**	**3**	**4**
Frequency (Hz)		1.70	5.09	7.92	/
Damping ratio (%)		2.24	0.61	1.82	/
SMS	***RSG4***	0.505	1.000	1.000	/
	RSG3	0.607	0.551	-0.553	/
	RSG2	0.934	-0.069	-0.806	/
	RSG1	1.000	-0.729	0.762	/

Table 7.30 Modal parameters of *Dcase_ANA* using RSGs measurements

Mode		1	2	3	4
Frequency (Hz)		1.63	5.01	/	/
Damping ratio (%)		1.79	0.85	/	/
SMS	***RSG4***	0.437	1.000	/	/
	RSG3	0.535	0.550	/	/
	RSG2	1.000	-0.031	/	/
	RSG1	0.868	-0.779	/	/

Table 7.31 Modal parameters of *Dcase_AAB* using RSGs measurements

Mode		**1**	**2**	**3**	**4**
Frequency (Hz)		1.68	5.03	/	/
Damping ratio (%)		2.98	0.33	/	/
SMS	***RSG4***	0.510	1.000	/	/
	RSG3	0.688	0.621	/	/
	RSG2	0.947	-0.083	/	/
	RSG1	1.000	-0.763	/	/

Table 7.32 Modal parameters of *Dcase_AAN* using RSGs measurements

Mode		**1**	**2**	**3**	**4**
Frequency (Hz)		1.63	4.81	7.79	/
Damping ratio (%)		3.04	0.18	2.27	/
SMS	***RSG4***	0.504	1.000	1.000	/
	RSG3	0.929	0.922	-0.548	/
	RSG2	0.947	-0.149	-0.523	/
	RSG1	1.000	-0.964	0.443	/

Table 7.33 Modal parameters of *Dcase_BBA* using RSGs measurements

Mode		**1**	**2**	**3**	**4**
Frequency (Hz)		1.62	4.88	7.74	/
Damping ratio (%)		2.42	2.03	1.04	/
SMS	***RSG4***	0.454	1.000	1.000	/
	RSG3	0.648	0.684	-0.395	/
	RSG2	0.871	-0.050	-0.729	/
	RSG1	1.000	-0.845	0.662	/

Table 7.34 Modal parameters of *Dcase_BNA* using RSGs measurements

Mode		**1**	**2**	**3**	**4**
Frequency (Hz)		1.60	4.90	7.52	/
Damping ratio (%)		1.72	1.36	2.01	/
SMS	***RSG4***	0.437	1.000	1.000	/
	RSG3	0.623	0.704	-0.259	/
	RSG2	1.000	-0.097	-0.985	/
	RSG1	0.872	-0.784	0.745	/

Table 7.35 Modal parameters of *Dcase_NBA* using RSGs measurements

Mode		**1**	**2**	**3**	**4**
Frequency (Hz)		1.58	4.76	7.61	/
Damping ratio (%)		1.56	0.56	3.84	/
SMS	***RSG4***	0.428	1.000	1.000	/
	RSG3	0.638	0.780	-0.525	/
	RSG2	0.852	0.051	-0.974	/
	RSG1	1.000	-0.927	0.921	/

Table 7.36 Modal parameters of *Dcase_NNA* using RSGs measurements

Mode		**1**	**2**	**3**	**4**
Frequency (Hz)		1.55	4.72	7.39	9.65
Damping ratio (%)		0.79	0.77	0.90	1.74
SMS	***RSG4***	0.420	1.000	0.929	-0.614
	RSG3	0.627	0.869	-0.207	1.000
	RSG2	0.966	-0.023	-1.000	-0.652
	RSG1	1.000	-0.887	0.696	0.277

Table 7.37 Modal parameters of *Dcase_BAB* using RSGs measurements

Mode		**1**	**2**	**3**	**4**
Frequency (Hz)		1.63	4.90	7.89	10.08
Damping ratio (%)		2.52	0.55	1.40	2.79
SMS	***RSG4***	0.452	1.000	1.000	-0.728
	RSG3	0.617	0.686	-0.582	1.000
	RSG2	0.870	-0.048	-0.689	-0.810
	RSG1	1.000	-0.780	0.652	0.263

Table 7.38 Modal parameters of *Dcase_BAN* using RSGs measurements

Mode		**1**	**2**	**3**	**4**
Frequency (Hz)		1.59	4.72	7.80	/
Damping ratio (%)		2.62	0.35	1.18	/
SMS	***RSG4***	0.446	1.000	1.000	/
	RSG3	0.843	0.960	-0.503	/
	RSG2	0.881	-0.080	-0.525	/
	RSG1	1.000	-0.975	0.486	/

Table 7.39 Modal parameters of *Dcase_NAB* using RSGs measurements

Mode		**1**	**2**	**3**	**4**
Frequency (Hz)		1.60	4.84	7.74	/
Damping ratio (%)		1.51	0.71	1.44	/
SMS	***RSG4***	0.421	1.000	1.000	/
	RSG3	0.586	0.641	-0.432	/
	RSG2	0.838	0.027	-0.734	/
	RSG1	1.000	-0.832	0.571	/

Table 7.40 Modal parameters of *Dcase_NAN* using RSGs measurements

Mode		**1**	**2**	**3**	**4**
Frequency (Hz)		1.56	4.63	7.68	/
Damping ratio (%)		1.37	0.02	1.12	/
SMS	***RSG4***	0.419	0.936	1.000	/
	RSG3	0.797	0.937	-0.398	/
	RSG2	0.846	0.055	-0.549	/
	RSG1	1.000	-1.000	0.438	/

Table 7.41 Modal parameters of *Dcase_ABB* using RSGs measurements

Mode		**1**	**2**	**3**	**4**
Frequency (Hz)		1.68	5.02	7.90	/
Damping ratio (%)		2.30	0.17	2.93	/
SMS	***RSG4***	0.503	1.000	1.000	/
	RSG3	0.687	0.618	-0.404	/
	RSG2	0.939	-0.094	-0.698	/
	RSG1	1.000	-0.738	0.646	/

Table 7.42 Modal parameters of *Dcase_ABN* using RSGs measurements

Mode		**1**	**2**	**3**	**4**
Frequency (Hz)		1.64	4.83	7.77	/
Damping ratio (%)		2.04	0.26	0.93	/
SMS	***RSG4***	0.510	1.000	1.000	/
	RSG3	0.939	0.894	-0.532	/
	RSG2	0.946	-0.145	-0.531	/
	RSG1	1.000	-0.906	0.463	/

Table 7.43 Modal parameters of *Dcase_ANB* using RSGs measurements

Mode		**1**	**2**	**3**	**4**
Frequency (Hz)		1.62	4.91	7.69	/
Damping ratio (%)		1.58	0.73	3.62	/
SMS	***RSG4***	0.439	1.000	0.986	/
	RSG3	0.598	0.659	-0.336	/
	RSG2	1.000	-0.033	-1.000	/
	RSG1	0.872	-0.841	0.759	/

Table 7.44 Modal parameters of *Dcase_ANN* using RSGs measurements

Mode		**1**	**2**	**3**	**4**
Frequency (Hz)		1.57	4.75	7.58	9.29
Damping ratio (%)		1.53	0.30	1.49	1.84
SMS	***RSG4***	0.429	1.000	1.000	-0.780
	RSG3	0.808	0.956	-0.442	1.000
	RSG2	1.000	-0.085	-0.792	-0.854
	RSG1	0.878	-0.919	0.654	0.312

Table 7.45 Modal parameters of *Dcase_BBB* using RSGs measurements

Mode		**1**	**2**	**3**	**4**
Frequency (Hz)		1.62	4.87	7.82	/
Damping ratio (%)		2.28	0.65	2.28	/
SMS	***RSG4***	0.443	1.000	1.000	/
	RSG3	0.628	0.687	-0.409	/
	RSG2	0.875	-0.027	-0.812	/
	RSG1	1.000	-0.822	0.770	/

Table 7.46 Modal parameters of *Dcase_BBN* using RSGs measurements

Mode		**1**	**2**	**3**	**4**
Frequency (Hz)		1.58	4.72	7.76	/
Damping ratio (%)		2.12	0.29	0.86	/
SMS	***RSG4***	0.440	1.000	1.000	/
	RSG3	0.823	0.991	-0.530	/
	RSG2	0.875	-0.081	-0.541	/
	RSG1	1.000	-0.956	0.496	/

Table 7.47 Modal parameters of *Dcase_NBB* using RSGs measurements

Mode		**1**	**2**	**3**	**4**
Frequency (Hz)		1.60	4.82	7.60	/
Damping ratio (%)		0.80	0.29	1.37	/
SMS	***RSG4***	0.429	1.000	1.000	/
	RSG3	0.604	0.696	-0.398	/
	RSG2	0.791	-0.036	-0.789	/
	RSG1	1.000	-0.837	0.576	/

Table 7.48 Modal parameters of *Dcase_BNN* using RSGs measurements

Mode		**1**	**2**	**3**	**4**
Frequency (Hz)		1.54	4.63	7.58	/
Damping ratio (%)		1.13	0.13	1.64	/
SMS	***RSG4***	0.425	0.981	1.000	/
	RSG3	0.799	0.983	-0.343	/
	RSG2	1.000	-0.032	-0.806	/
	RSG1	0.972	-1.000	0.633	/

Table 7.49 Modal parameters of *Dcase_NNB* using RSGs measurements

Mode		**1**	**2**	**3**	**4**
Frequency (Hz)		1.56	4.81	7.38	/
Damping ratio (%)		0.41	0.60	0.68	/
SMS	***RSG4***	0.414	1.000	0.942	/
	RSG3	0.573	0.659	-0.195	/
	RSG2	0.977	0.018	-1.000	/
	RSG1	1.000	-0.831	0.679	/

Table 7.50 Modal parameters of *Dcase_NNN* using RSGs measurements

Mode		**1**	**2**	**3**	**4**
Frequency (Hz)		1.53	4.64	7.34	/
Damping ratio (%)		0.31	0.12	0.63	/
SMS	***RSG4***	0.412	1.000	1.000	/
	RSG3	0.776	0.985	-0.296	/
	RSG2	0.992	-0.038	-0.864	/
	RSG1	1.000	-0.986	0.624	/

7.2.3 Modal Data of the Specimen Extracted from the FBG Sensors Measurements

As mentioned, FBG sensors have much better immunity to electro-magnetic interference; therefore, the noise effect when using FBG sensors is much smaller than when using RSGs. This has been first discussed in section 6.6.2, and will be further examined here. Following the same procedure when analyzing the RSGs measurements, the FBG sensors measurements are also analyzed to obtain the corresponding strain mode shapes information. Only the records from the FBG sensors on Channel 1 (i.e. FBG1 to FBG8) are used for modal analysis. The identified results obtained from the FBG sensors measurements for each simulated deterioration case are shown in Tables 7.51 to 7.75.

Before discussing the identified results, certain important things should be noted in advance. Although the rate for sampling the FBG sensors measurements is set to be 106Hz, the sampling rate did not stay constant during the test; it fluctuated around 106Hz. While the sampling rate for the input excitation is set to be constant 200Hz.

Since the ANNSI model needs the structural output responses and the input excitation for identifying the structural modal parameters, the input excitation need to be re-sampled due to the incoordination in sampling rates of the structural responses and input excitation. The input excitations for each deterioration case are re-sampled with 106Hz by using linear interpolation method before they are used for modal analysis. Theoretically, no matter what measurements (such as structural displacement, velocity, acceleration, and strain) are used for modal analysis, the identified modal frequencies for the same structure should be identical to each other. Subject to the problems of fluctuant sampling rate and data re-sampling, however, the identified modal parameters extracted from the FBG sensors measurements could be different to those based on the RSGs measurements. Even though, this phenomenon would not influence the objective of structural health monitoring.

According to the identifications, it is found that:

(1) Generally, the signal noise increases the difficulty of system identification. More explicitly, since the signals from the FBG sensors are cleaner than those from the RSGs, the order needed for the ANNSI model when using the FBG sensors measurements is much lesser than when using the RSGs measurements. The number of order needed for identifying the lower modes is quite small. This feature is attractive in on-line system identification because smaller order implies quicker identification.

(2) Unlike the identification results obtained from the RSGs measurements, four modes in most cases can be successfully identified by using the FBG sensors measurements. This feature is advantaged in the cases of higher modes are needed. For example, it has been seen that the changes in lower

modes for slight deterioration scenarios are not distinct enough to indicate deterioration, while the changes in higher modes, though their accuracies are lower, are distinguishable to signify possible deterioration.

Table 7.51 Modal parameters of *AAA* using FBG sensors measurements

Mode		**1**	**2**	**3**	**4**
Frequency (Hz)		1.71	5.29	8.37	10.66
Damping ratio (%)		2.89	2.26	2.43	3.13
SMS	***FBG8***	0.416	-0.996	-0.962	-0.901
	FBG7	-0.406	1.000	1.000	1.000
	FBG6	0.635	-0.678	0.517	0.348
	FBG5	-0.594	0.650	-0.481	-0.265
	FBG4	0.814	0.087	0.751	-0.587
	FBG3	-0.793	-0.128	-0.828	0.767
	FBG2	1.000	0.710	-0.733	0.769
	FBG1	-0.966	-0.859	0.789	-0.600

Table 7.52 Modal parameters of *Dcase_BAA* using FBG sensors measurements

Mode		**1**	**2**	**3**	**4**
Frequency (Hz)		1.70	5.21	8.18	/
Damping ratio (%)		2.57	3.85	2.06	/
SMS	***FBG8***	0.404	-1.000	-0.973	/
	FBG7	-0.397	0.994	1.000	/
	FBG6	0.623	-0.736	0.548	/
	FBG5	-0.583	0.702	-0.522	/
	FBG4	0.802	0.080	0.787	/
	FBG3	-0.782	-0.107	-0.864	/
	FBG2	1.000	0.731	-0.601	/
	FBG1	-0.946	-0.883	0.665	/

Table 7.53 Modal parameters of *Dcase_NAA* using FBG sensors measurements

Mode		**1**	**2**	**3**	**4**
Frequency (Hz)		1.65	4.97	8.11	/
Damping ratio (%)		1.76	0.89	0.95	/
SMS	***FBG8***	0.340	-1.000	-0.991	/
	FBG7	-0.334	0.999	1.000	/
	FBG6	0.553	-0.788	0.486	/
	FBG5	-0.519	0.759	-0.450	/
	FBG4	0.699	-0.086	0.831	/
	FBG3	-0.674	0.071	-0.905	/
	FBG2	1.000	0.820	-0.687	/
	FBG1	-0.957	-0.959	0.715	/

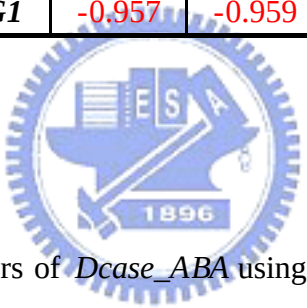

Table 7.54 Modal parameters of *Dcase_ABA* using FBG sensors measurements

Mode		**1**	**2**	**3**	**4**
Frequency (Hz)		1.73	5.35	8.27	/
Damping ratio (%)		2.88	0.54	1.96	/
SMS	***FBG8***	0.401	-1.000	-0.932	/
	FBG7	-0.392	0.999	0.978	/
	FBG6	0.538	-0.588	0.571	/
	FBG5	-0.497	0.550	-0.510	/
	FBG4	0.832	-0.018	0.919	/
	FBG3	-0.817	-0.051	-1.000	/
	FBG2	1.000	0.584	-0.753	/
	FBG1	-0.967	-0.771	0.816	/

Table 7.55 Modal parameters of *Dcase_ANA* using FBG sensors measurements

Mode		**1**	**2**	**3**	**4**
Frequency (Hz)		1.67	5.19	/	/
Damping ratio (%)		1.82	0.77	/	/
SMS	***FBG8***	0.391	-1.000	/	/
	FBG7	-0.387	1.000	/	/
	FBG6	0.542	-0.629	/	/
	FBG5	-0.489	0.593	/	/
	FBG4	1.000	-0.105	/	/
	FBG3	-0.986	0.069	/	/
	FBG2	0.941	0.668	/	/
	FBG1	-0.926	-0.843	/	/

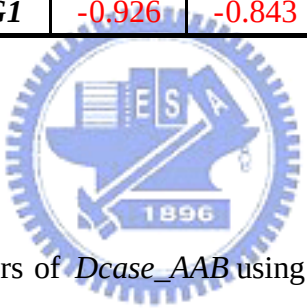

Table 7.56 Modal parameters of *Dcase_AAB* using FBG sensors measurements

Mode		**1**	**2**	**3**	**4**
Frequency (Hz)		1.71	5.21	8.27	10.48
Damping ratio (%)		2.91	1.26	3.78	2.25
SMS	***FBG8***	0.408	-0.998	-0.944	-0.548
	FBG7	-0.398	1.000	1.000	0.616
	FBG6	0.612	-0.699	0.673	0.960
	FBG5	-0.566	0.667	-0.629	-1.000
	FBG4	0.841	0.063	0.856	-0.838
	FBG3	-0.826	-0.081	-0.960	0.872
	FBG2	1.000	0.664	-0.522	0.347
	FBG1	-0.964	-0.828	0.628	-0.497

Table 7.57 Modal parameters of *Dcase_AAN* using FBG sensors measurements

Mode		**1**	**2**	**3**	**4**
Frequency (Hz)		1.64	4.96	7.98	10.00
Damping ratio (%)		3.28	0.92	1.99	2.56
SMS	***FBG8***	0.414	-1.000	-0.962	-0.291
	FBG7	-0.392	0.982	1.000	0.340
	FBG6	0.803	-0.990	0.686	1.000
	FBG5	-0.757	0.970	-0.662	-0.983
	FBG4	0.829	0.092	0.635	-0.836
	FBG3	-0.825	-0.110	-0.721	0.875
	FBG2	1.000	0.818	-0.446	0.257
	FBG1	-0.967	-0.975	0.489	-0.263

Table 7.58 Modal parameters of *Dcase_BBA* using FBG sensors measurements

Mode		**1**	**2**	**3**	**4**
Frequency (Hz)		1.64	5.09	8.04	10.52
Damping ratio (%)		2.41	3.64	2.62	2.86
SMS	***FBG8***	0.366	-0.998	-0.968	-0.443
	FBG7	-0.358	1.000	1.000	0.557
	FBG6	0.576	-0.754	0.521	1.000
	FBG5	-0.533	0.723	-0.469	-0.955
	FBG4	0.783	-0.090	0.854	-0.525
	FBG3	-0.767	0.078	-0.940	0.639
	FBG2	1.000	0.704	-0.696	0.373
	FBG1	-0.976	-0.851	0.753	-0.526

Table 7.59 Modal parameters of *Dcase_BNA* using FBG sensors measurements

Mode		**1**	**2**	**3**	**4**
Frequency (Hz)		1.65	5.19	7.75	10.00
Damping ratio (%)		1.29	3.81	1.50	1.57
SMS	***FBG8***	0.399	-1.000	-0.795	-0.607
	FBG7	-0.393	0.998	0.818	0.656
	FBG6	0.632	-0.747	0.338	0.963
	FBG5	-0.575	0.710	-0.299	-1.000
	FBG4	0.997	0.073	0.893	-0.901
	FBG3	-1.000	-0.087	-1.000	0.914
	FBG2	0.975	0.706	-0.607	0.004
	FBG1	-0.949	-0.871	0.617	-0.009

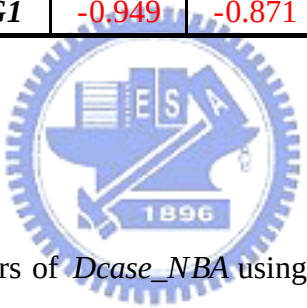

Table 7.60 Modal parameters of *Dcase_NBA* using FBG sensors measurements

Mode		**1**	**2**	**3**	**4**
Frequency (Hz)		1.63	4.90	7.86	/
Damping ratio (%)		1.07	0.74	2.30	/
SMS	***FBG8***	0.342	-0.981	-0.966	/
	FBG7	-0.336	0.979	0.998	/
	FBG6	0.554	-0.841	0.344	/
	FBG5	-0.513	0.808	-0.304	/
	FBG4	0.749	-0.102	0.886	/
	FBG3	-0.733	0.098	-1.000	/
	FBG2	1.000	0.860	-0.732	/
	FBG1	-0.968	-1.000	0.778	/

Table 7.61 Modal parameters of *Dcase_NNA* using FBG sensors measurements

Mode		**1**	**2**	**3**	**4**
Frequency (Hz)		1.59	4.79	7.60	9.96
Damping ratio (%)		0.34	2.18	1.25	1.79
SMS	***FBG8***	0.344	-0.961	-0.779	-0.583
	FBG7	-0.337	0.954	0.800	0.620
	FBG6	0.567	-0.922	0.262	0.977
	FBG5	-0.517	0.894	-0.217	-1.000
	FBG4	0.872	-0.075	0.900	-0.841
	FBG3	-0.873	0.082	-1.000	0.854
	FBG2	1.000	0.855	-0.494	0.104
	FBG1	-0.977	-1.000	0.505	-0.126

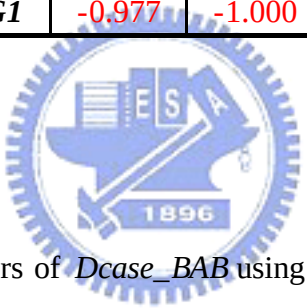

Table 7.62 Modal parameters of *Dcase_BAB* using FBG sensors measurements

Mode		**1**	**2**	**3**	**4**
Frequency (Hz)		1.66	5.05	8.09	10.35
Damping ratio (%)		2.31	1.56	1.36	1.47
SMS	***FBG8***	0.365	-1.000	-0.976	-0.630
	FBG7	-0.357	0.999	1.000	0.666
	FBG6	0.551	-0.741	0.502	1.000
	FBG5	-0.510	0.716	-0.479	-0.999
	FBG4	0.783	-0.070	0.687	-0.834
	FBG3	-0.760	-0.072	-0.768	0.870
	FBG2	1.000	0.722	-0.644	0.331
	FBG1	-0.970	-0.880	0.682	-0.355

Table 7.63 Modal parameters of *Dcase_BAN* using FBG sensors measurements

Mode		**1**	**2**	**3**	**4**
Frequency (Hz)		1.63	4.85	8.03	10.02
Damping ratio (%)		2.24	0.34	0.42	3.17
SMS	***FBG8***	0.375	-0.961	-0.974	-0.804
	FBG7	-0.355	0.941	1.000	0.855
	FBG6	0.733	-0.987	0.452	0.699
	FBG5	-0.694	0.968	-0.443	-0.739
	FBG4	0.785	0.057	0.437	-0.940
	FBG3	-0.773	-0.067	-0.503	1.000
	FBG2	1.000	0.851	-0.468	0.693
	FBG1	-0.969	-1.000	0.488	-0.788

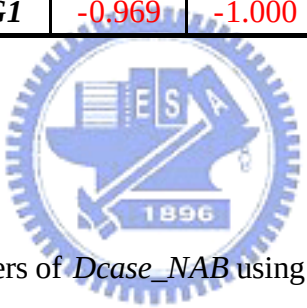

Table 7.64 Modal parameters of *Dcase_NAB* using FBG sensors measurements

Mode		**1**	**2**	**3**	**4**
Frequency (Hz)		1.64	4.91	8.05	10.38
Damping ratio (%)		0.94	2.77	0.85	3.01
SMS	***FBG8***	0.336	-1.000	-0.970	-0.665
	FBG7	-0.331	0.999	1.000	0.707
	FBG6	0.515	-0.788	0.563	0.993
	FBG5	-0.477	0.754	-0.527	-1.000
	FBG4	0.744	-0.212	0.839	-0.867
	FBG3	-0.720	0.201	-0.927	0.910
	FBG2	1.000	0.786	-0.482	0.278
	FBG1	-0.964	-0.924	0.514	-0.350

Table 7.65 Modal parameters of *Dcase_NAN* using FBG sensors measurements

Mode		**1**	**2**	**3**	**4**
Frequency (Hz)		1.61	4.78	8.00	10.00
Damping ratio (%)		0.82	0.32	1.26	1.62
SMS	***FBG8***	0.346	-0.885	-0.970	-0.397
	FBG7	-0.327	0.865	1.000	0.439
	FBG6	0.681	-0.933	0.549	1.000
	FBG5	-0.649	0.912	-0.536	-0.986
	FBG4	0.740	-0.066	0.512	-0.621
	FBG3	-0.725	0.071	-0.605	0.639
	FBG2	1.000	0.865	-0.475	0.347
	FBG1	-0.963	-1.000	0.490	-0.364

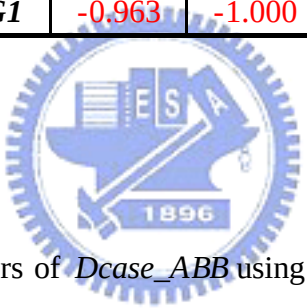

Table 7.66 Modal parameters of *Dcase_ABB* using FBG sensors measurements

Mode		**1**	**2**	**3**	**4**
Frequency (Hz)		1.71	5.22	8.22	10.47
Damping ratio (%)		2.31	1.15	2.24	1.93
SMS	***FBG8***	0.405	-1.000	-0.954	-0.265
	FBG7	-0.393	1.000	1.000	0.293
	FBG6	0.604	-0.695	0.614	0.986
	FBG5	-0.561	0.667	-0.571	-1.000
	FBG4	0.835	0.025	0.836	-0.630
	FBG3	-0.822	-0.066	-0.932	0.657
	FBG2	1.000	0.663	-0.612	0.158
	FBG1	-0.968	-0.827	0.646	-0.096

Table 7.67 Modal parameters of *Dcase_ABN* using FBG sensors measurements

Mode		**1**	**2**	**3**	**4**
Frequency (Hz)		1.66	4.97	8.04	9.88
Damping ratio (%)		1.67	0.66	0.46	2.00
SMS	***FBG8***	0.423	-1.000	-0.954	-0.279
	FBG7	-0.401	0.983	1.000	0.300
	FBG6	0.815	-0.977	0.628	0.978
	FBG5	-0.767	0.960	-0.609	-1.000
	FBG4	0.827	0.102	0.568	-0.784
	FBG3	-0.824	-0.127	-0.646	0.812
	FBG2	1.000	0.824	-0.440	0.174
	FBG1	-0.964	-0.986	0.473	-0.161

Table 7.68 Modal parameters of *Dcase_ANB* using FBG sensors measurements

Mode		**1**	**2**	**3**	**4**
Frequency (Hz)		1.66	5.03	7.82	10.21
Damping ratio (%)		1.67	2.48	3.82	3.84
SMS	***FBG8***	0.396	-1.000	-0.920	-0.724
	FBG7	-0.390	0.996	0.941	0.695
	FBG6	0.607	-0.748	0.373	1.000
	FBG5	-0.551	0.719	-0.354	-0.937
	FBG4	1.000	-0.096	0.899	-0.734
	FBG3	-0.989	0.079	-1.000	0.779
	FBG2	0.954	0.772	-0.807	0.685
	FBG1	-0.939	-0.938	0.834	-0.694

Table 7.69 Modal parameters of *Dcase_ANN* using FBG sensors measurements

Mode		**1**	**2**	**3**	**4**
Frequency (Hz)		1.62	4.87	7.85	9.68
Damping ratio (%)		1.29	0.64	1.54	1.64
SMS	***FBG8***	0.409	-0.958	-0.970	-0.755
	FBG7	-0.387	0.939	1.000	0.800
	FBG6	0.802	-0.981	0.359	0.981
	FBG5	-0.752	0.961	-0.335	-0.995
	FBG4	1.000	0.044	0.732	-0.976
	FBG3	-0.997	-0.045	-0.845	1.000
	FBG2	0.962	0.839	-0.555	0.300
	FBG1	-0.946	-1.000	0.533	-0.291

Table 7.70 Modal parameters of *Dcase_BBB* using FBG sensors measurements

Mode		**1**	**2**	**3**	**4**
Frequency (Hz)		1.67	5.05	8.08	10.26
Damping ratio (%)		2.14	1.37	1.38	2.03
SMS	***FBG8***	0.361	-1.000	-0.961	-0.442
	FBG7	-0.351	0.998	1.000	0.434
	FBG6	0.554	-0.748	0.560	1.000
	FBG5	-0.516	0.725	-0.524	-0.982
	FBG4	0.787	-0.037	0.858	-0.640
	FBG3	-0.769	0.016	-0.943	0.667
	FBG2	1.000	0.742	-0.526	0.169
	FBG1	-0.971	-0.898	0.567	-0.240

Table 7.71 Modal parameters of *Dcase_BBN* using FBG sensors measurements

Mode		**1**	**2**	**3**	**4**
Frequency (Hz)		1.62	4.88	8.02	9.97
Damping ratio (%)		1.91	0.48	0.97	2.79
SMS	***FBG8***	0.369	-0.970	-0.953	-0.793
	FBG7	-0.350	0.950	1.000	0.775
	FBG6	0.720	-0.989	0.635	0.904
	FBG5	-0.680	0.972	-0.612	-0.902
	FBG4	0.778	0.055	0.574	-0.944
	FBG3	-0.768	-0.070	-0.650	1.000
	FBG2	1.000	0.849	-0.555	0.880
	FBG1	-0.969	-1.000	0.575	-0.926

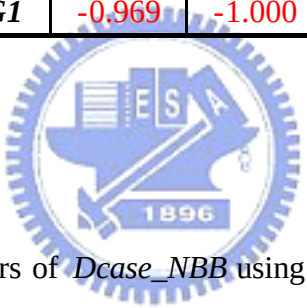

Table 7.72 Modal parameters of *Dcase_NBB* using FBG sensors measurements

Mode		**1**	**2**	**3**	**4**
Frequency (Hz)		1.65	4.92	7.92	10.32
Damping ratio (%)		0.63	1.27	0.89	1.66
SMS	***FBG8***	0.346	-1.000	-0.981	-0.568
	FBG7	-0.343	0.997	1.000	0.633
	FBG6	0.536	-0.801	0.437	1.000
	FBG5	-0.496	0.777	-0.389	-0.987
	FBG4	0.730	-0.113	0.789	-0.717
	FBG3	-0.700	0.100	-0.876	0.822
	FBG2	1.000	0.768	-0.675	0.275
	FBG1	-0.979	-0.909	0.685	-0.179

Table 7.73 Modal parameters of *Dcase_BNN* using FBG sensors measurements

Mode		**1**	**2**	**3**	**4**
Frequency (Hz)		1.58	4.76	7.78	9.59
Damping ratio (%)		0.42	0.74	1.09	0.89
SMS	***FBG8***	0.376	-0.922	-0.958	-0.618
	FBG7	-0.356	0.902	1.000	0.666
	FBG6	0.741	-0.981	0.506	1.000
	FBG5	-0.693	0.959	-0.462	-0.994
	FBG4	0.936	-0.031	0.814	-0.682
	FBG3	-0.932	0.031	-0.940	0.696
	FBG2	1.000	0.853	-0.676	0.490
	FBG1	-0.983	-1.000	0.704	-0.479

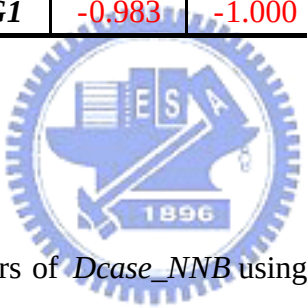

Table 7.74 Modal parameters of *Dcase_NNB* using FBG sensors measurements

Mode		**1**	**2**	**3**	**4**
Frequency (Hz)		1.60	4.88	7.63	/
Damping ratio (%)		0.27	2.58	0.66	/
SMS	***FBG8***	0.338	-1.000	-0.946	/
	FBG7	-0.332	0.997	0.967	/
	FBG6	0.525	-0.869	0.252	/
	FBG5	-0.476	0.837	-0.214	/
	FBG4	0.875	-0.189	0.880	/
	FBG3	-0.870	0.196	-1.000	/
	FBG2	1.000	0.722	-0.743	/
	FBG1	-0.976	-0.843	0.743	/

Table 7.75 Modal parameters of *Dcase_NNN* using FBG sensors measurements

Mode		**1**	**2**	**3**	**4**
Frequency (Hz)		1.57	4.80	7.59	9.52
Damping ratio (%)		0.20	0.86	0.80	0.91
SMS	***FBG8***	0.349	-0.919	-0.979	-0.704
	FBG7	-0.329	0.897	1.000	0.783
	FBG6	0.688	-0.968	0.362	1.000
	FBG5	-0.644	0.949	-0.321	-0.973
	FBG4	0.879	-0.020	0.876	-0.919
	FBG3	-0.880	0.019	-0.988	0.951
	FBG2	1.000	0.860	-0.615	0.260
	FBG1	-0.973	-1.000	0.605	-0.267

7.3 Damage Detection With The Displacement-Based Modal Data

In the program, the experimental data are scheduled to be applied to the proposed damage diagnosis methods presented in Chapter 5. However, due to the following problems, the experimental data at this stage fail to be applied.

(1) The most difficult problem should be solved for all the model-based damage assessment methods is the inconsistency between the analytical model and real structure. As the structure becomes larger, thought it is possible, it is harder to make the analytical model close to the real structure. Due to this problem, most successful works limited to small-sized or simple structure (such as cantilever beam and truss structure). In this study, the analytical model was tried to modify according to the identified natural frequencies (Table 7.1). Although this can be achieved, the mode shapes produced by the modified analytical model are quite different from the identified ones.

Therefore, the analytical model is not reliable enough to be used to generate the training patterns (DLFs) for either the UFN or BPN.

(2) A feature of the UFN is that, with more training instances in the *instance base*, the accuracy becomes higher. This is predominant when using the UFN because the damage states for structures are numerous. In contrast, if the number of training instances is small, the performance of UFN could be inferior to that of BPN.

Although the proposed two-stage damage assessment method has not yet applied to the experimental data. There are other strategies, which will be introduced in Sections 7.4 and 7.5, are employed to diagnose the condition of the test structure. Once the suitable analytical model is generated, the model-based method will be used to enhance the diagnosis performance.

In the following, the experimental outputs (based on the acceleration measurements) from the tests are discussed.

7.3.1 Damage Indicators from the Displacement-Based Modal Data

First, damage indicators are tried to extract from the displacement-based modal data. The damage indicators that based on the displacement mode shapes are defined by the following equation.

$$\mathrm{CMS}^i = \frac{MS^i_{\mathrm{baseline}} - MS^i_{\mathrm{damaged}}}{MS^i_{\mathrm{baseline}}} \times 100\% \tag{7.1}$$

in which CMS^i denotes the changes in the ith displacement mode shapes; the MS^i_{baseline}

and MS^{i}_{damaged} represent the *i*th displacement mode shapes of the intact and deteriorated structures, respectively.

The CMSs of the 24 deterioration cases are classified by their deterioration class and are diagramed in Figures 7.7 to 7.13. Note that, only the CMSs of the 1st mode (i.e. *i*=1) were presented in those figures. According to those figures, some interesting findings are discussed.

(1) The effect of replacing the SCs-A with SCs-B at only one story is not so significant to be identified from the CMS. For example, the CMSs for the cases of slight deterioration scenario, *Dcase_BAA*, *Dcase_ABA*, and *Dcase_AAB*, are below 5% (Figures 7.7 to 7.9). Therefore, the detection of structural deterioration using CMS for slight deterioration case may be unreliable. A more sensitive deterioration indicator that capable of detecting the slight deterioration in a structure should be developed.

(2) As the deterioration extent increased, the CMS becomes larger and related to the deterioration location for the single-site deterioration cases (Figures 7.7 to 7.9).

(3) The CMS of multiple-site deterioration cases is somehow combinations of the CMS of single-site deterioration cases. For example, deteriorated at k_1 resulting in enlargement of displacement mode shape at all sensing stations (such as *Dcase_NAA* in Figure 7.7), while deteriorated at k_3 causing reduction of displacement mode shape at the stations A1 and A2 (such as *Dcase_AAN* in Figure 7.9); consequently, though the overall deterioration extent of *Dcase_NAN* is higher than *Dcase_NAA* or *Dcase_AAN*, the CMS

of *Dcase_NAN* is smaller than that of *Dcase_NAA* or *Dcase_AAN*. Therefore, it is much harder to diagnose the deterioration location by directly using the CMS in multiple-site deterioration cases.

(4) Due to the finding (1), the CMS for *Dcase_AAN* (Figure 7.9) is similar to the one for *Dcase_ABN* (Figure 7.12). Likewise, the CMS for *Dcase_NAA* (Figure 7.9) is similar to the one of *Dcase_NAB* (Figure 7.12). This observation confirms the requirement for involving the fuzzy concept in the damage detection of a structure.

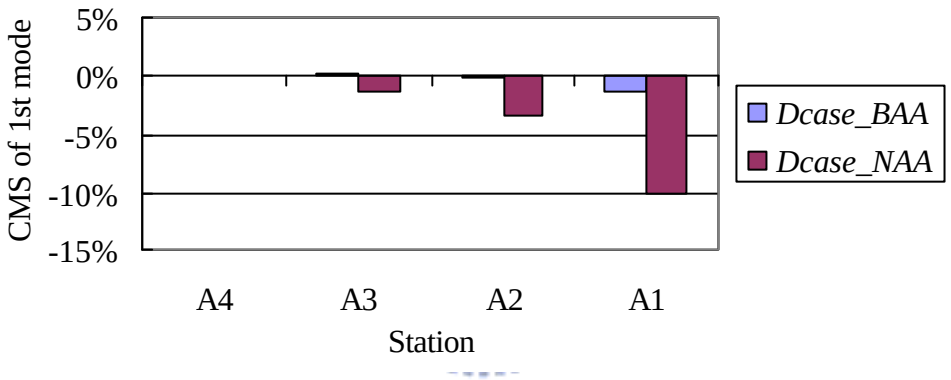

Figure 7.7 CMS for *Dclass_k*$_1$

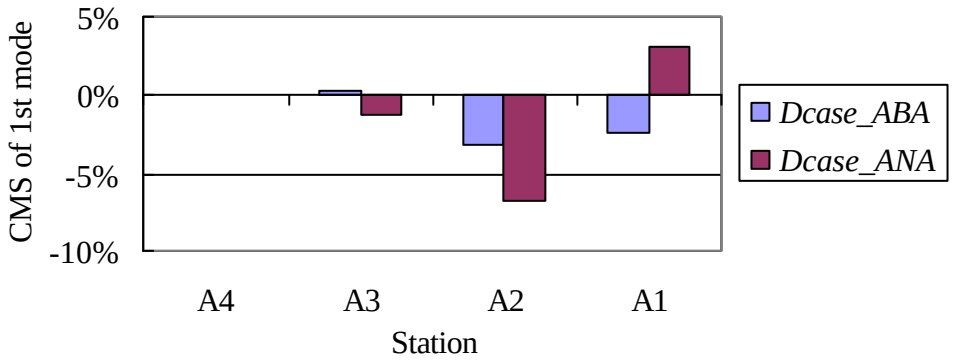

Figure 7.8 CMS for *Dclass_k*$_2$

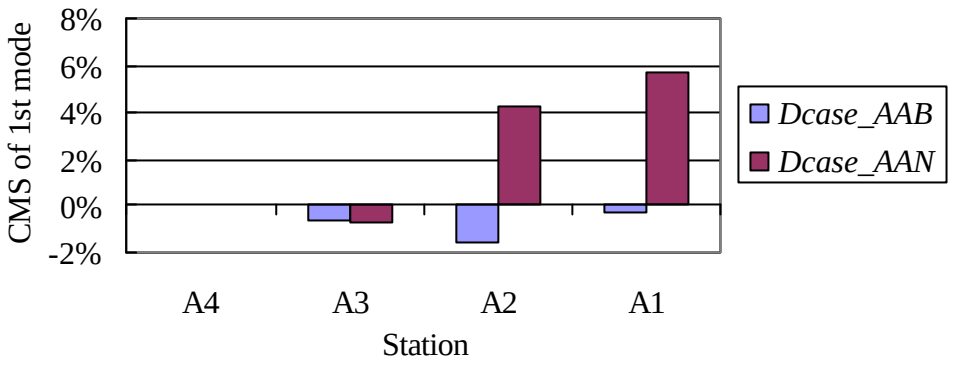

Figure 7.9 CMS for *Dclass_k*$_3$

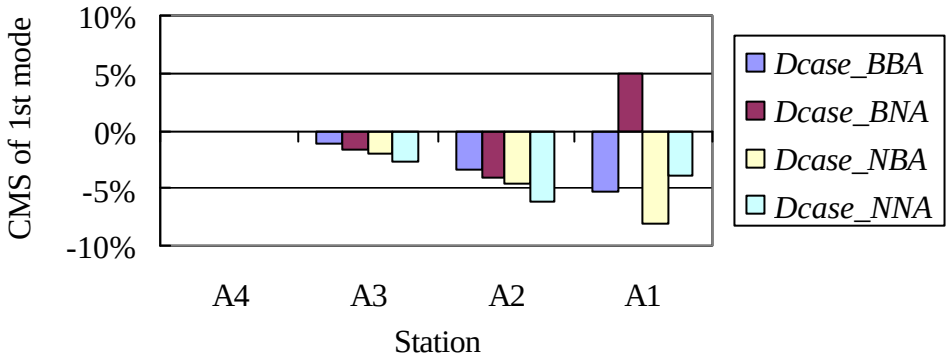

Figure 7.10 CMS for *Dclass_k*$_1$&*k*$_2$

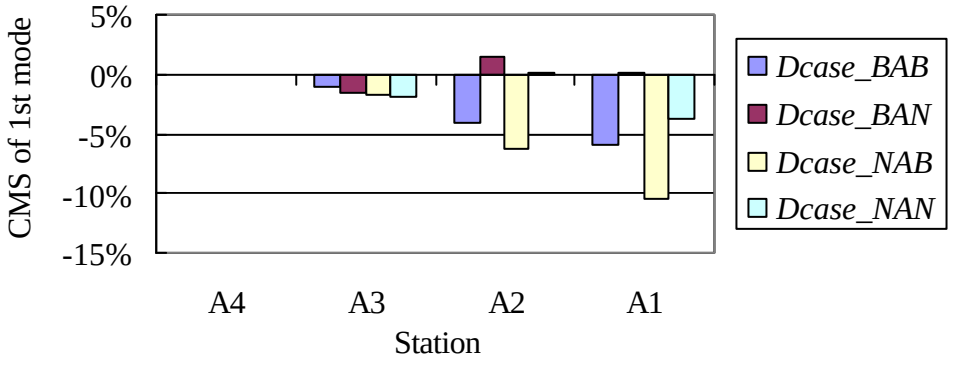

Figure 7.11 CMS for *Dclass_k*$_1$&*k*$_3$

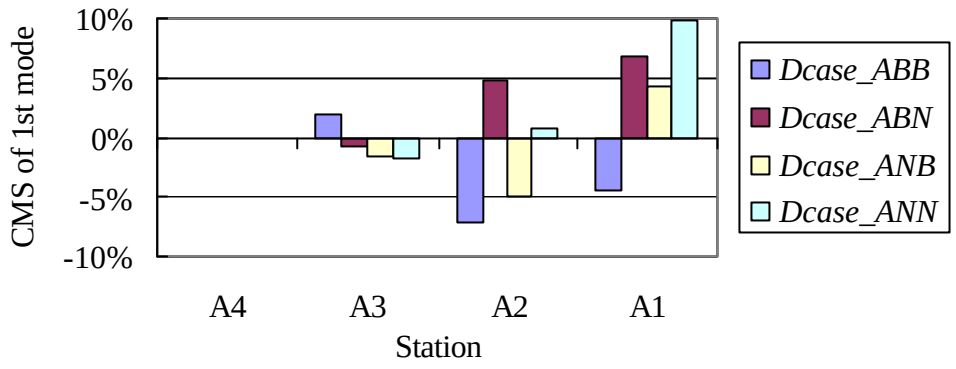

Figure 7.12 CMS for *Dclass_*k_2&k_3

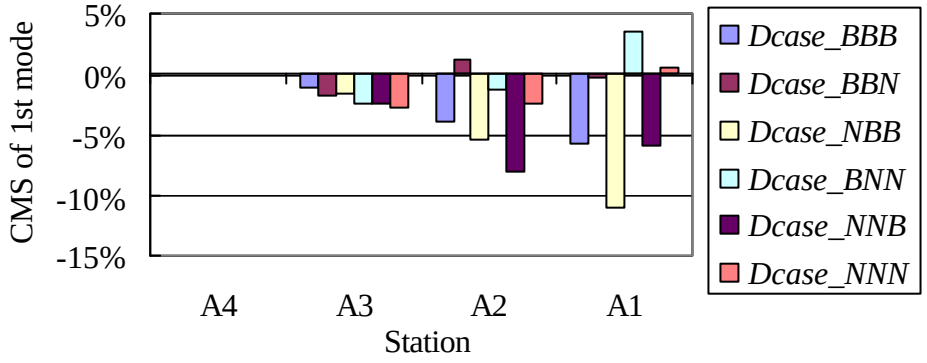

Figure 7.13 CMS for *Dclass_*k_1&k_2&k_3

7.3.2 Monitoring of Degradation Development in Story Stiffness Based on the Modal Data

In a health monitoring system, frequently monitoring of structural condition is the key to provide reliable diagnosis on the structure. Therefore, the degradation development in story stiffness is discussed herein. The deterioration cases of *Dcase_BAA*, *Dcase_NAA*, *Dcase_NBA*, *Dcase_NNA*, *Dcase_NNB*, and *Dcase_NNN* are selected to simulate the degradation of the structure. The development of

degradation is assumed to start from single site (at the 1st story) to multiple sites (at the 1st, 2nd, and 3rd stories).

The variations of the natural frequencies are used to monitor the conditions of the test structure. Figure 7.14 shows the variations of the natural frequencies during simulated degradation. Evidently, the natural frequency of the structure decreased as the structure was deteriorated. Though a slight change in the structure can not be explicitly identified in one single episode, such as from *AAA* to *Dcase_BAA* or from *Dcase_NNA* to *Dcase_NNB*, it is possible to find out the gradual damage of the structure through sustained monitoring.

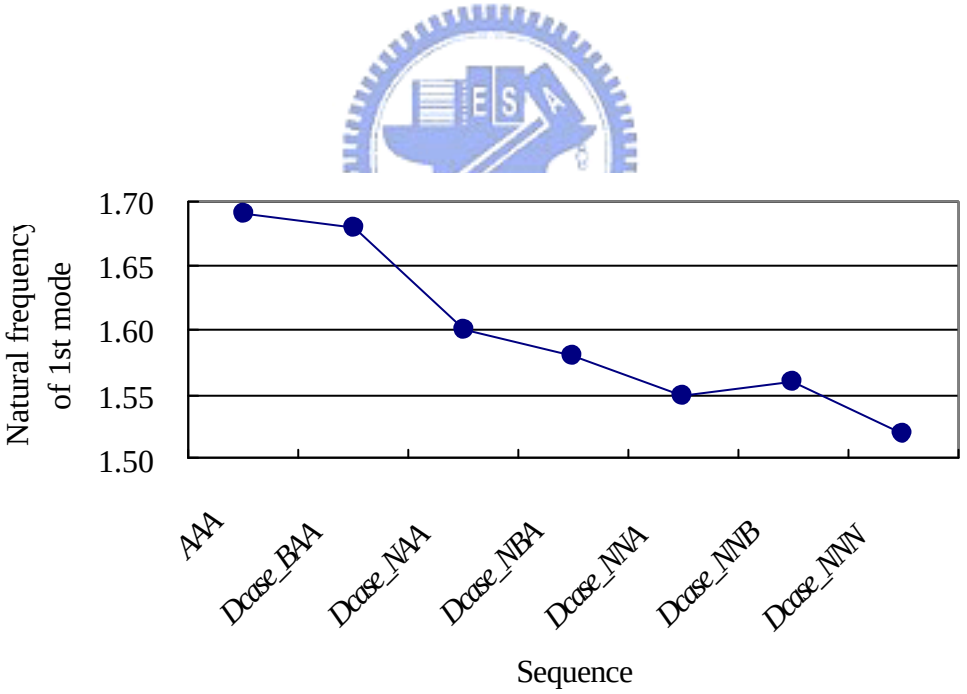

Figure 7.14 Variations of the natural frequencies in the structure of degradation

7.4 Damage Detection With The Strain-Based Modal Data

The rational for using strain mode shapes for structural diagnosis is as follows. Structural damage will be always followed by stress and strain redistribution. The changes in the stresses and strains will be highest in the locality of the damage, and hence the damaged site can be located. Consequently, the strain mode shapes are adopted as a basis for damage detection of structures.

7.4.1 Extraction of the Damage Indicators

To extract the damage indicators from the strain mode shapes, the strain mode shapes obtained in previous sections were reprocessed with two operations. In the first operation, the strain mode shapes were normalized with respect to the station at the column of the 4th story (i.e. RSG4 if the SMS from RSG is used, and FBG8 if the SMS from FBG is used). Secondly, the changes in strain mode shapes (CSMS) are calculated according to the following equation.

$$\mathrm{CSMS}^i = \frac{SMS^i_{\mathrm{baseline}} - SMS^i_{\mathrm{damaged}}}{SMS^i_{\mathrm{baseline}}} \times 100\% \qquad (7.1)$$

in which the $SMS^i_{\mathrm{baseline}}$ and SMS^i_{damaged} represent the ith strain mode shapes of the intact and deteriorated structures. Theoretically, deterioration increases the amplitude of strain vibration, and results in enlargement of strain mode shape. Therefore, the computed CSMS should be negative if the deterioration existed in the structure.

7.4.2 Damage Indicators Obtained from the RSGs Measurements

It is found that the CSMS of the 1st mode is related to the location of the structural damage. As a result, only this mode will be appear in later discussions. The CSMSs of the 24 deterioration cases are classified by their deterioration class and are diagramed in Figures 7.15 to 7.21. According the results shown in those figures, certain discussions are made.

(1) Compare with the CMS (Figures 7.7 to 7.13), the CSMS of the structure is more sensitive to the structural deterioration. Moreover, the location of deterioration can be reflected by the sensing stations with larger value of CSMS. For examples, the structure of *Dcase_NAA* was deteriorated at the 1st story columns, the maximum CSMS happened to the station RSG1 which was attached to the 1st story column; likewise, the structure of *Dcase_NNA* was both deteriorated at the 1st and 2nd story columns, the larger CSMSs happened to the stations RSG1 and RSG2 which were attached to the 1st and 2nd story columns. Therefore, the CSMS could be a deterioration indicator for identifying the location of the structural deterioration.

(2) Clear differences between the CSMSs for each deterioration class could be found if the structural deterioration is severe enough. Unfortunately, the CSMSs for the low-level deterioration cases, such as *Dcase_BAA*, *Dcase_ABA*, and *Dcase_AAB*, seem not large enough to be used for locating the structural deterioration.

(3) If the CSMSs for each deterioration cases were passed the threshold of -10% to classify the existence of deterioration in the structure, the identified

deterioration locations basing on the CSMS and the threshold for each case are listed in the following table (Table 7.76). According to this table, the identified results in most cases are satisfactory.

Table 7.76 Possible deterioration location identified by using the CSMS and with a threshold of -10% (RSG measurements)

Case	Actual deterioration location	Identified deterioration location
Dcase_BAA	k_1	none
Dcase_NAA	k_1	k_1
Dcase_ABA	k_2	none
Dcase_ANA	k_2	k_2
Dcase_AAB	k_3	none
Dcase_AAN	k_3	k_3
Dcase_BBA	k_1 & k_2	k_1 & k_2
Dcase_BNA	k_1 & k_2	k_2
Dcase_NBA	k_1 & k_2	k_1 & k_2
Dcase_NNA	k_1 & k_2	k_1 & k_2
Dcase_BAB	k_1 & k_3	k_1 & k_2
Dcase_BAN	k_1 & k_3	k_1 & k_2 & k_3
Dcase_NAB	k_1 & k_3	k_1 & k_2
Dcase_NAN	k_1 & k_3	k_1 & k_2 & k_3
Dcase_ABB	k_2 & k_3	none
Dcase_ABN	k_2 & k_3	k_3
Dcase_ANB	k_2 & k_3	k_2
Dcase_ANN	k_2 & k_3	k_2 & k_3
Dcase_BBB	k_1 & k_2 & k_3	none
Dcase_BBN	k_1 & k_2 & k_3	k_1 & k_2 & k_3
Dcase_NBB	k_1 & k_2 & k_3	k_1
Dcase_BNN	k_1 & k_2 & k_3	k_1 & k_2 & k_3
Dcase_NNB	k_1 & k_2 & k_3	k_1 & k_2
Dcase_NNN	k_1 & k_2 & k_3	k_1 & k_2 & k_3

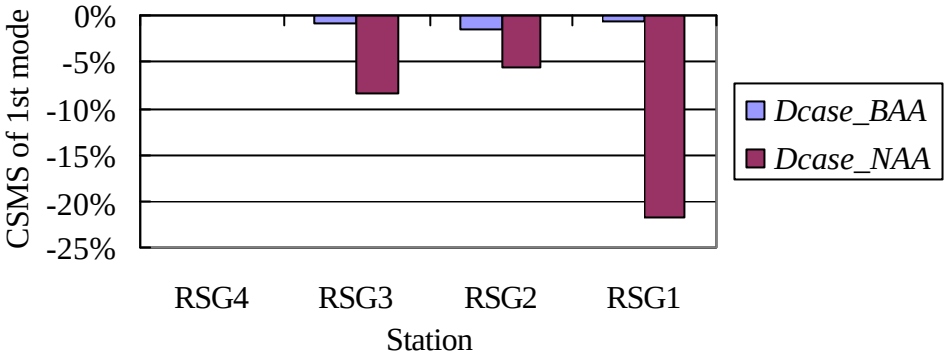

Figure 7.15 CSMS for *Dclass_k*$_1$ (RSGs measurements)

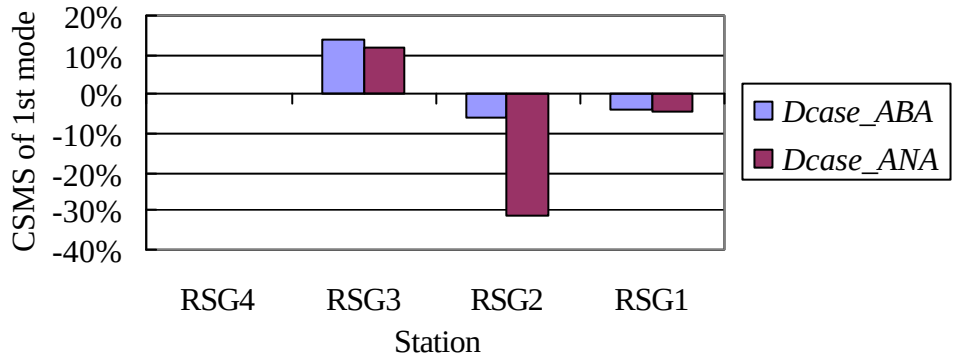

Figure 7.16 CSMS for *Dclass_k*$_2$ (RSGs measurements)

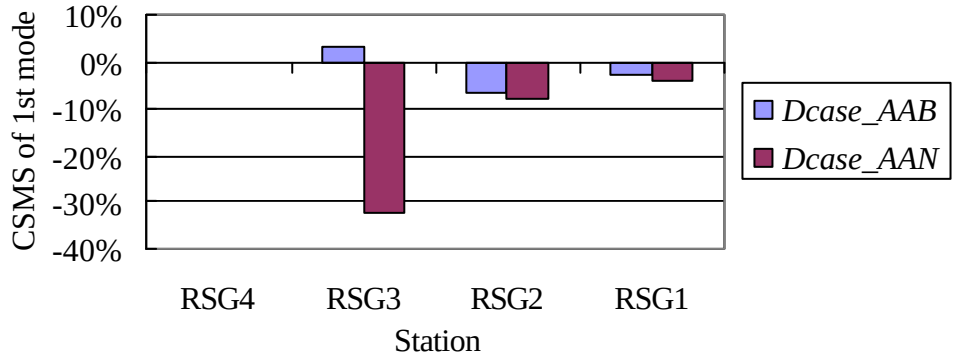

Figure 7.17 CSMS for *Dclass_k*$_3$ (RSGs measurements)

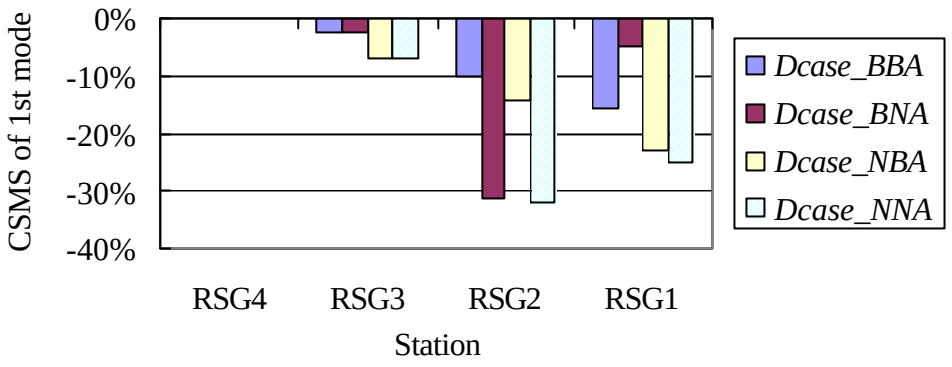

Figure 7.18 CSMS for *Dclass_*k_1&k_2 (RSGs measurements)

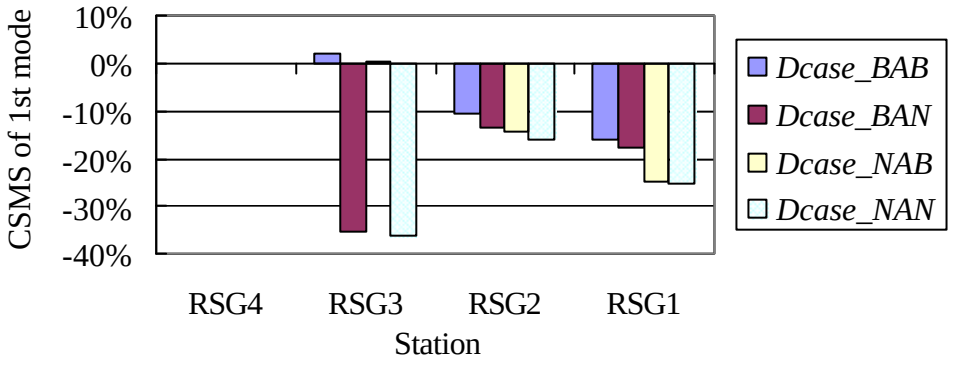

Figure 7.19 CSMS for *Dclass_*k_1&k_3 (RSGs measurements)

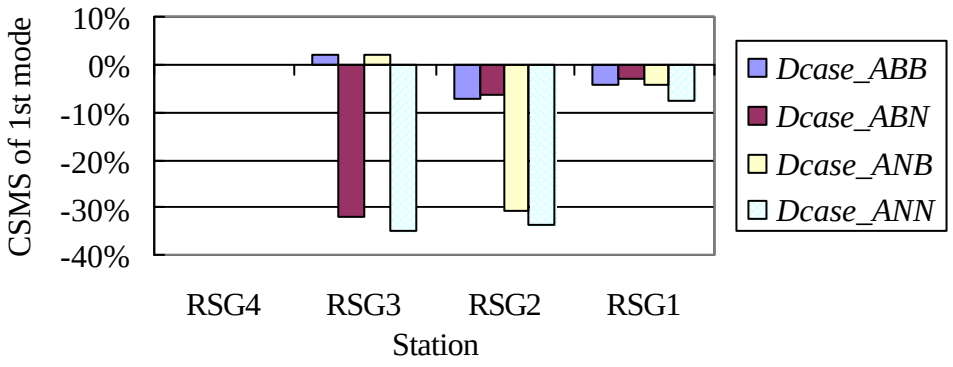

Figure 7.20 CSMS for *Dclass_*k_2&k_3 (RSGs measurements)

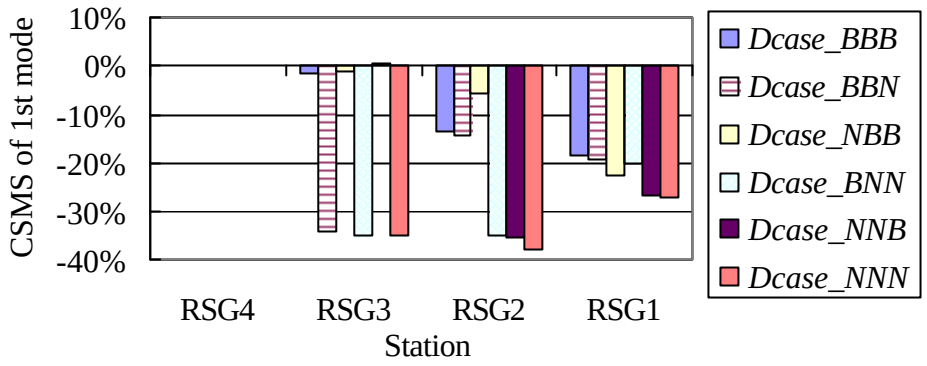

Figure 7.21 CSMS for *Dclass_*k_1&k_2&k_3 (RSGs measurements)

7.4.3 Damage Indicator Obtained from the FBG sensors Measurements

To obtain the CSMSs of each deteriorated case from the FBG sensors meaurements, the strain mode shapes obtained previously (Tables 7.51 to 7.75) were reprocessed with the forgoing two operations. Note that, the strain mode shapes are normalized with respect to FBG8. Again, only the strain mode shape of the 1st mode was used to calculate the CSMS. The CSMSs of the 24 deterioration cases are classified by their deterioration class and are diagramed in Figures 7.22 to 7.28. There are two FBG sensors were attached to each story column (as shown in Figure 6.6). Compare with the RSGs, the FBG sensors provide more monitoring information to assess the structural condition.

If the CSMSs for each deterioration case were passed the threshold of -10%, the identified deterioration locations basing on the CSMS and the threshold for each case are listed in Table 7.77. Note that, if the value of CSMS at any one of the two FBG stations of each story passes the threshold, the corresponding location will be selected

as candidate for possible deterioration. For example, if the values of CSMS at stations FBG3 and FBG4 (which were installed at the 2nd story) are -8% and -12%, the columns at the 2nd story will be treated as deterioration positive since the CSMS at FBG4 exceeds -10%. According to this table, the identified results that based on the FBG sensors measurements are satisfactory in most cases. Furthermore, they also show better diagnosis than the results that based on the RSGs measurements (Table 7.76).

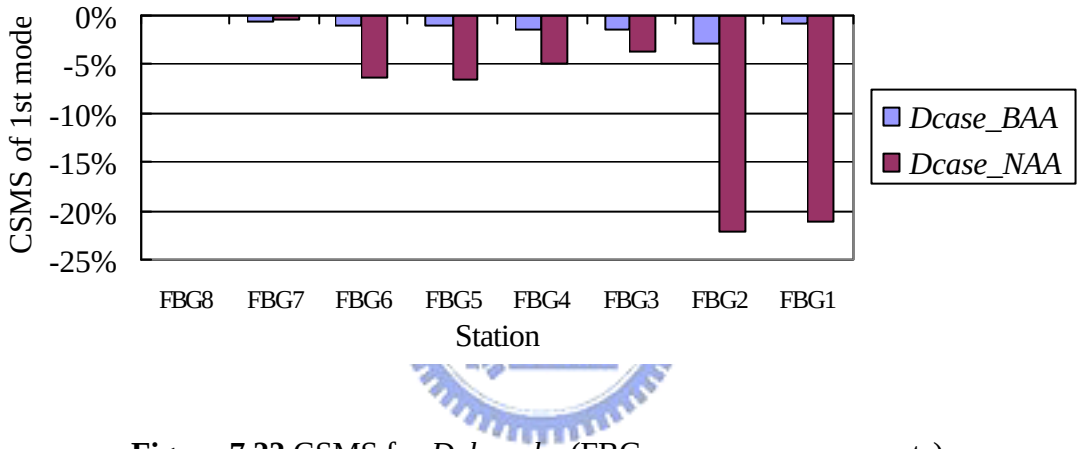

Figure 7.22 CSMS for *Dclass_k*$_1$ (FBG sensors measurements)

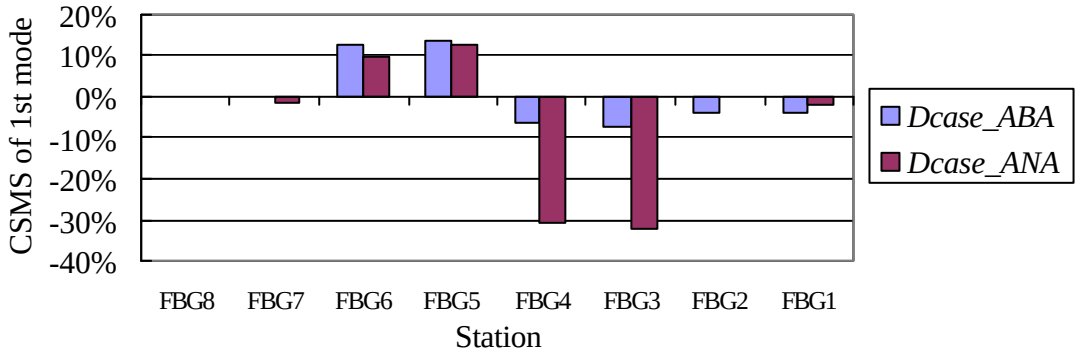

Figure 7.23 CSMS for *Dclass_k*$_2$ (FBG sensors measurements)

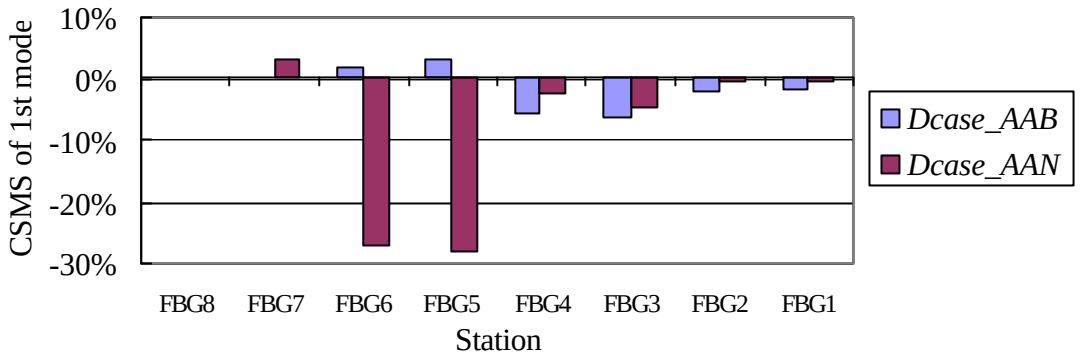

Figure 7.24 CSMS for *Dclass_k*$_3$ (FBG sensors measurements)

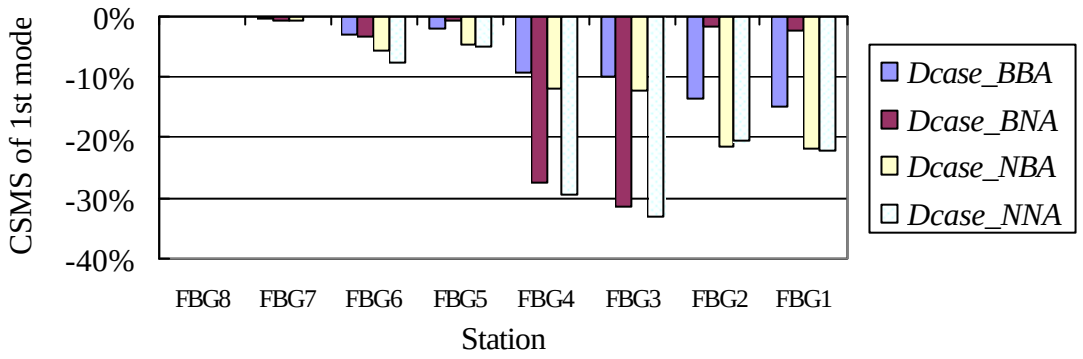

Figure 7.25 CSMS for *Dclass_k*$_1$&*k*$_2$ (FBG sensors measurements)

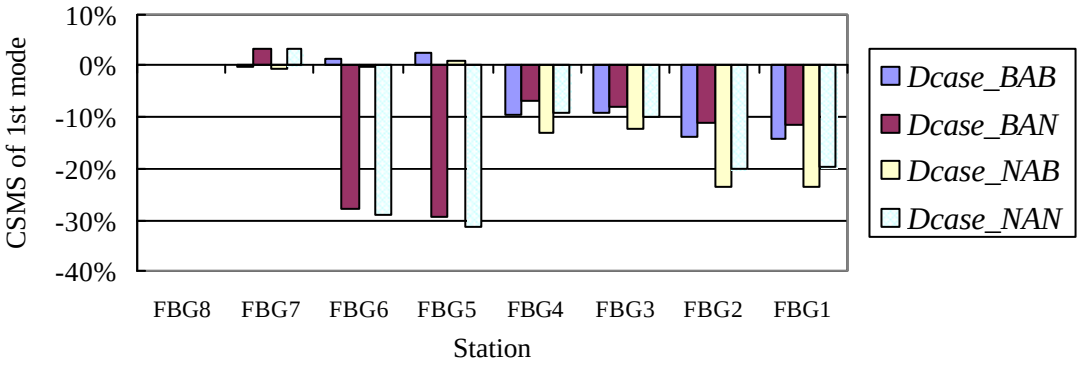

Figure 7.26 CSMS for *Dclass_k*$_1$&*k*$_3$ (FBG sensors measurements)

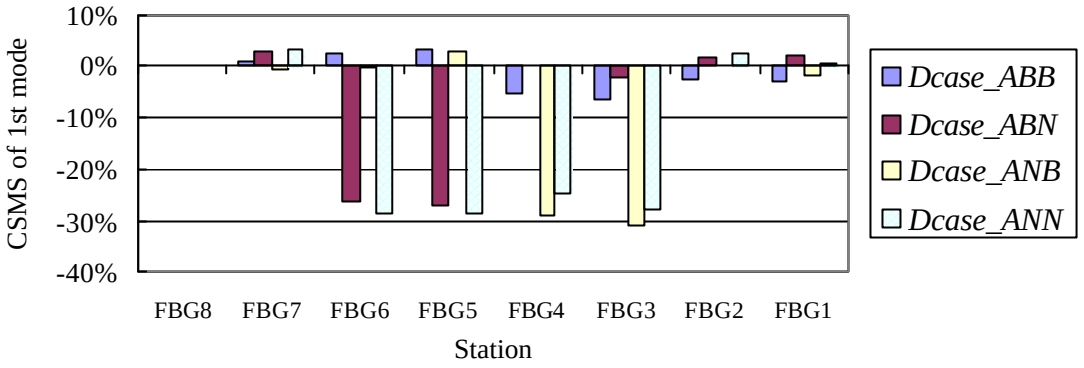

Figure 7.27 CSMS for *Dclass_*k_2&k_3 (FBG sensors measurements)

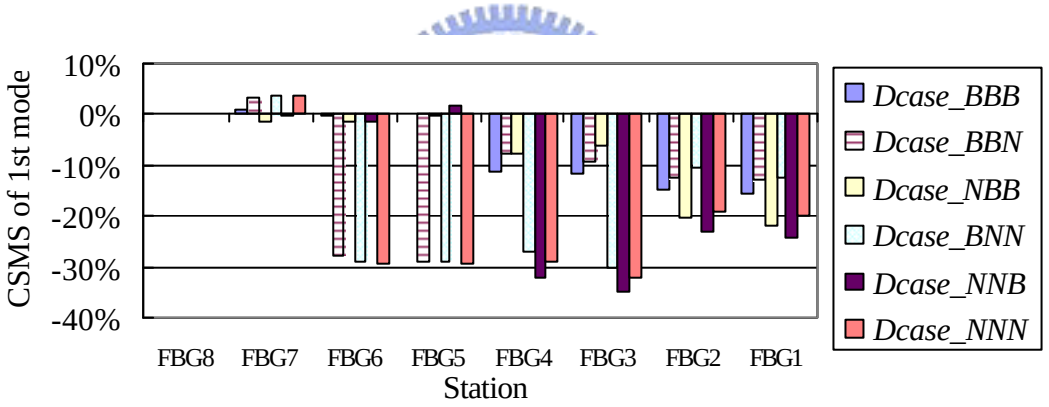

Figure 7.28 CSMS for *Dclass_*k_1&k_2&k_3 (FBG sensors measurements)

Table 7.77 Possible deterioration location identified by using the CSMS and with a threshold of -10% (FBG sensors measurements)

Case	Actual deterioration location	Identified deterioration location
Dcase_BAA	k_1	none
Dcase_NAA	k_1	k_1
Dcase_ABA	k_2	none
Dcase_ANA	k_2	k_2
Dcase_AAB	k_3	none
Dcase_AAN	k_3	k_3
Dcase_BBA	k_1 & k_2	k_1 & k_2
Dcase_BNA	k_1 & k_2	k_2
Dcase_NBA	k_1 & k_2	k_1 & k_2
Dcase_NNA	k_1 & k_2	k_1 & k_2
Dcase_BAB	k_1 & k_3	k_1
Dcase_BAN	k_1 & k_3	k_1 & k_3
Dcase_NAB	k_1 & k_3	k_1 & k_2
Dcase_NAN	k_1 & k_3	k_1 & k_3
Dcase_ABB	k_2 & k_3	none
Dcase_ABN	k_2 & k_3	k_3
Dcase_ANB	k_2 & k_3	k_2
Dcase_ANN	k_2 & k_3	k_2 & k_3
Dcase_BBB	k_1 & k_2 & k_3	k_1 & k_2
Dcase_BBN	k_1 & k_2 & k_3	k_1 & k_3
Dcase_NBB	k_1 & k_2 & k_3	k_1
Dcase_BNN	k_1 & k_2 & k_3	k_1 & k_2 & k_3
Dcase_NNB	k_1 & k_2 & k_3	k_1 & k_2
Dcase_NNN	k_1 & k_2 & k_3	k_1 & k_2 & k_3

7.4.4 Further Discussions on the FBG Sensors and RSGs

According to the results and discussions in previous sections, it is seen that the noise effect on the FBG sensors is much smaller than on the RSGs which feature makes the system identification easier. Moreover, due to the problems of fluctuant sampling rate and data re-sampling when using the FBG sensors measurements, though the identified frequencies from the FBG sensors and RSGs measurements are not the same, the diagnostic results that based on the damage indicator, CSMS, are quite similar. All of these indicate that FBG sensors have their own characteristics to replace traditional RSGs.

In this research, the structural deterioration is limited to story level (i.e. the deterioration is reflected by the change in story stiffness); few RSGs are enough to provide the deterioration information (such CSMS). Due to the complexity of real structures, however, only few sensors are definitely not enough to provide reliable diagnosis on the structural condition. Under this situation, the total number and mass of wires connected to RSGs, and the electro-magnetic interference will be significant. Consequently, in addition to the feature of much smaller noise effect, the distinguishing advantages of much less mass and great capacity of multiplexing a large number of sensors along a single fiber link make FBG sensors a promising sensing unit for health monitoring of practical structures. In the most ideal condition, the FBG sensors can be arranged to distribute on the whole structure to act as biological nerves. Under this situation, the structural health monitoring would be easier and more reliable. Though it is nowadays impractical, it is possible to implement this task in the future. If this is not achievable, monitoring critical members or zones is the alternative way to make the health monitoring of structures more effective. No matter what situation is in,

placing more sensors at right places is the key to successful damage detection and health monitoring.

7.5 Damage Detection With The Monitoring Networks

In Sections 4.5.3 and 4.5.4, the global and decentralized monitoring networks were preliminarily examined by either laboratory or numerical example, respectively. The results had shown their potentials for applying to the practical situations. In this section, they are further investigated by the experimental data obtained from the conducted shaking table tests on a four-story steel frame structure. Acceleration measurements as well as strain measurements from FBG sensors are used for investigations.

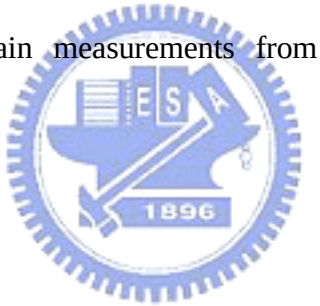

7.5.1 Health Monitoring Using Global Monitoring Networks

For health monitoring purpose, the MAN that had been trained by the measurements from an intact structure is employed to play the role of monitoring unit. The way of monitoring is basing on the idea that depicted in Figure 4.7. The trained MAN should be capable of generating the system outputs from it within a tolerable error range if the structure does not change. On the contrary, if the structural characteristics of target structure changed significantly, the trained MAN for the intact structure will no more suitable for representing the current state of the structure; as a result, the generated outputs from the trained MAN will differ from the measured responses from the deteriorated structure.

The health monitoring approach of using global monitoring network is applied to the acceleration and strain measurements, respectively. Notably, the strain measurements used in this section are the ones observed from the FBG sensors (FBG1 to FBG8). Start from the acceleration measurements, each set of measurements of the 24 deterioration cases is fed into the MAN trained by the AAA_acc measurement. The relative changes in prediction error are shown in Figure 7.29. Note that, throughout this section, the prediction error is based on MAE which was shown in equation (4.38). Since the global monitoring network provides global view on structural condition, the prediction error is derived by calculating the average of MAEs of every DOF. It is seen from Figure 7.29 that the structural deterioration indeed increases the prediction error of the monitoring network. However, it is not easy to affirm structural deterioration from comparing any two of data, especially when the deterioration is not significant. Therefore, continuous monitoring on a structure is essential. To investigate this situation, the relative changes in prediction errors of the six cases for simulating the degradation development in a structure, which has been mentioned in Section 7.3.2, are picked out and presented in Figure 7.30. According to this figure, the prediction errors can reflect the possibility of the existence of structural deterioration. In addition, the gradual increment in prediction error indicates the degradation development in the structure. Again by this result, the essentiality of sustained monitoring on a structure for reliable diagnosis is validated.

Figure 7.29 Relative increments in prediction error in all deterioration cases based on acceleration measurements

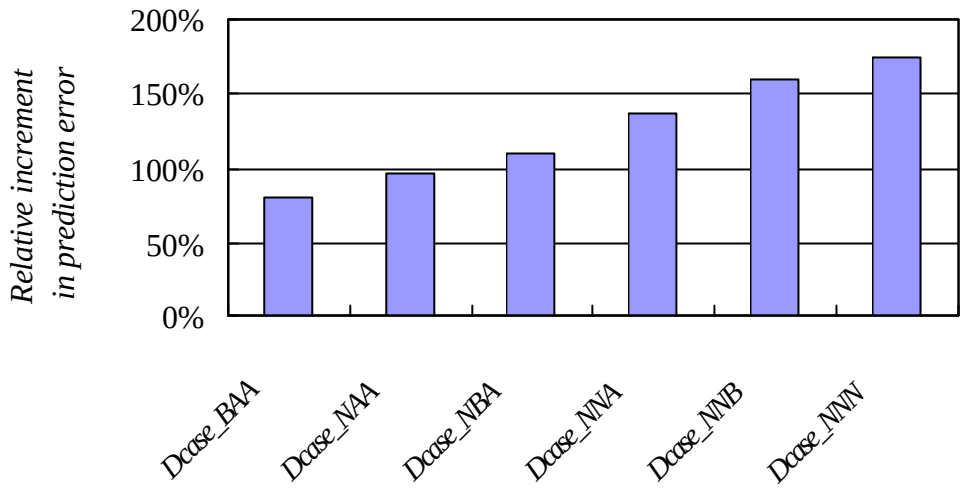

Figure 7.30 Relative increments in prediction error in the structure of degradation based on acceleration measurements

If the FBG sensors measurements are used for health monitoring by using global monitoring network, the prediction errors of the 24 deterioration cases are depicted in Figure 7.31. Likewise, the results of the six cases for simulating the degradation development in a structure are shown in Figure 7.32. Compare the results of these two figures with those of Figures 7.29 and 7.30, the results show the similar trend while the structure was deteriorated though there were slight difference existed between them. Moreover, the increments in prediction error of strain measurements are larger than those of acceleration in serious deterioration cases. For examples, the relative increments in prediction error of acceleration and strain measurements for *Dcase_NAA* are within 100% and beyond 300%, respectively; the maximum values in Figures 7.29 and 7.31 are about 175% and 870%, respectively.

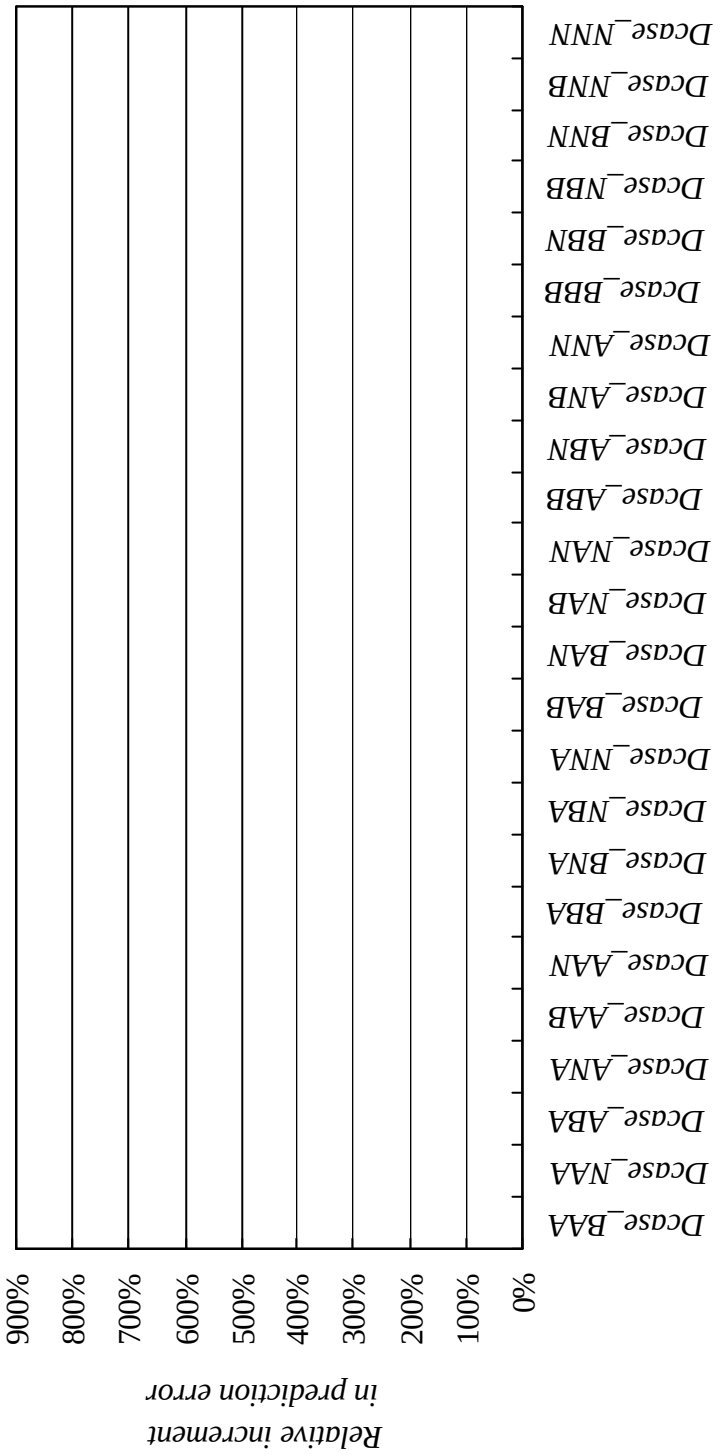

Figure 7.31 Relative increments in prediction error in all deterioration cases based on strain measurements (from FBG sensors)

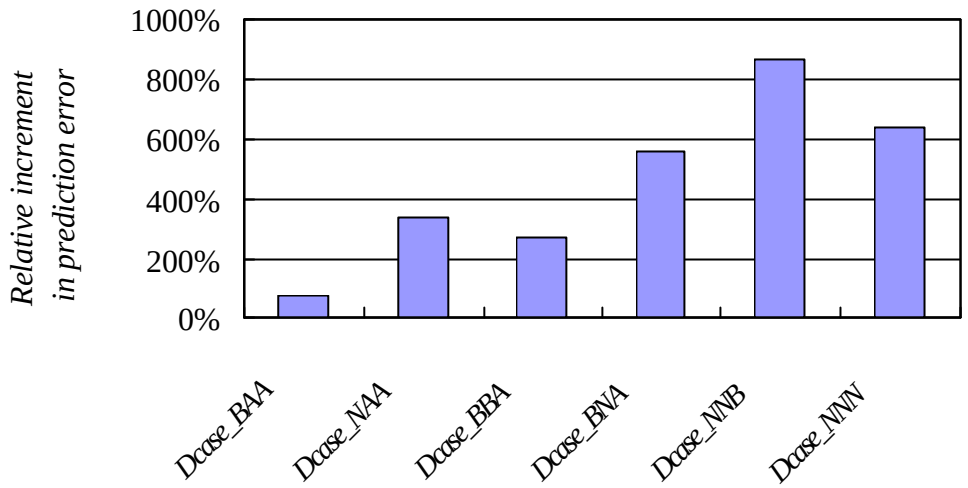

Figure 7.32 Relative increments in prediction error in the structure of degradation based on strain measurements (from FBG sensors)

7.5.2 Health Monitoring Using Decentralized Monitoring Networks

When using decentralized monitoring networks for health monitoring purpose, they should be trained in advance. Once more, the acceleration measurements are investigated first. There are four decentralized monitoring networks need to be trained by the observations for the healthy structure. They are denoted as Net_1, Net_2, Net_3, and Net_4 according to the DOFs they attempt to monitor. According to the formulas shown in equation (4.37), the training input-output data for each decentralized monitoring network is determined. After these four networks were trained, they are fed with the measurements of the 24 deterioration cases to monitor the variations in prediction errors. Then the decision roles for detecting deterioration location, which were discussed in Sections 4.5.2 and listed in Table 4.4, can be applied based on the

monitored prediction errors from each decentralized monitoring network.

Figures 7.33 to 7.39 present the radar diagrams of the relative increments in prediction errors of each decentralized monitoring network for various deterioration classes. According to these figures, some interesting appearances are observed.

(1) The results between each deterioration class are not distinguishable in the cases of slight deterioration; nevertheless, they do indicate clear difference between each single-site deterioration class in the cases of much severe deterioration. For examples, the decentralized monitoring network, Net_1, produces the maximum prediction error in the case of *Dcase_NAA*; likewise, Net_2 and Net_3 cause the maximum prediction errors in the cases *Dcase_ANA* and *Dcase_AAN*, respectively.

(2) The severity of the structural deterioration can be reflected by the incremental prediction errors of the decentralized monitoring networks.

(3) The deterioration location can be roughly identified if the decision roles for detecting deterioration location are adopted.

Based on the results and foregoing discussions, the decentralized monitoring networks seem a potential and promising tool for the local health monitoring of structures.

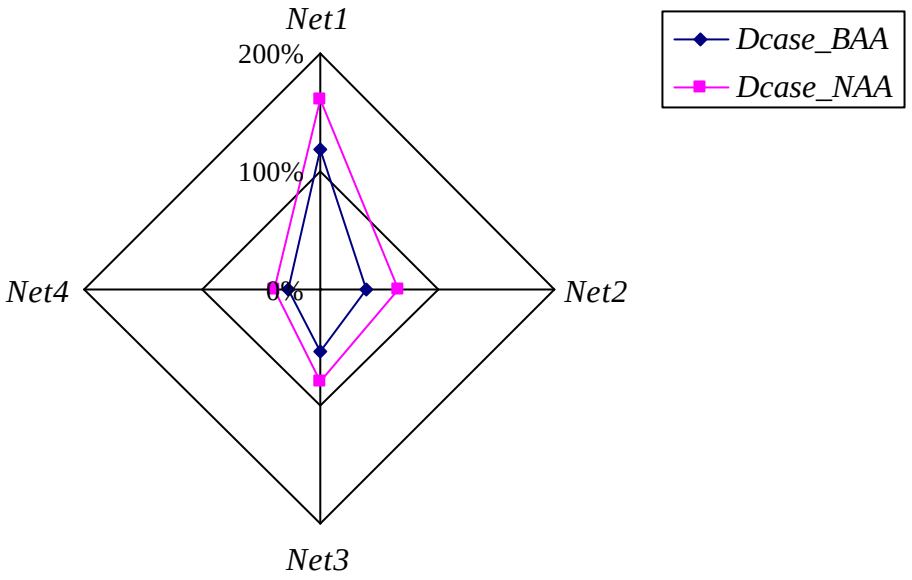

Figure 7.33 Relative increments in prediction error of each decentralized monitoring network for *Dclass_k*$_1$ (using acceleration measurements)

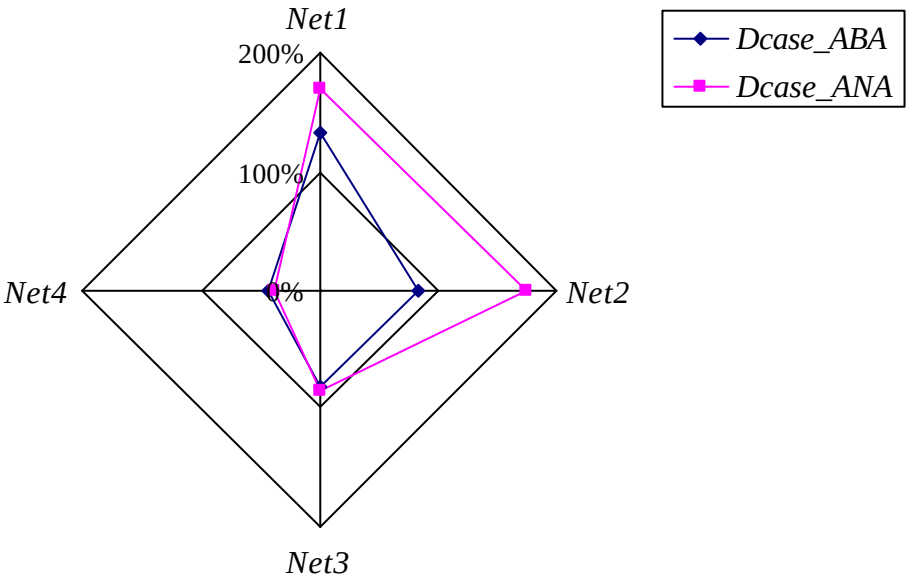

Figure 7.34 Relative increments in prediction error of each decentralized monitoring network for *Dclass_k*$_2$ (using acceleration measurements)

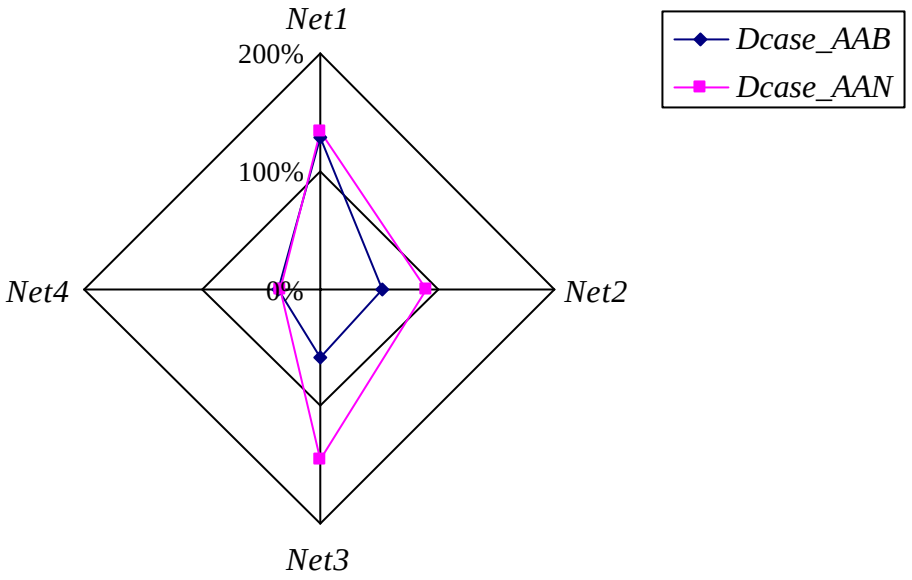

Figure 7.35 Relative increments in prediction error of each decentralized monitoring network for *Dclass_*k_3 (using acceleration measurements)

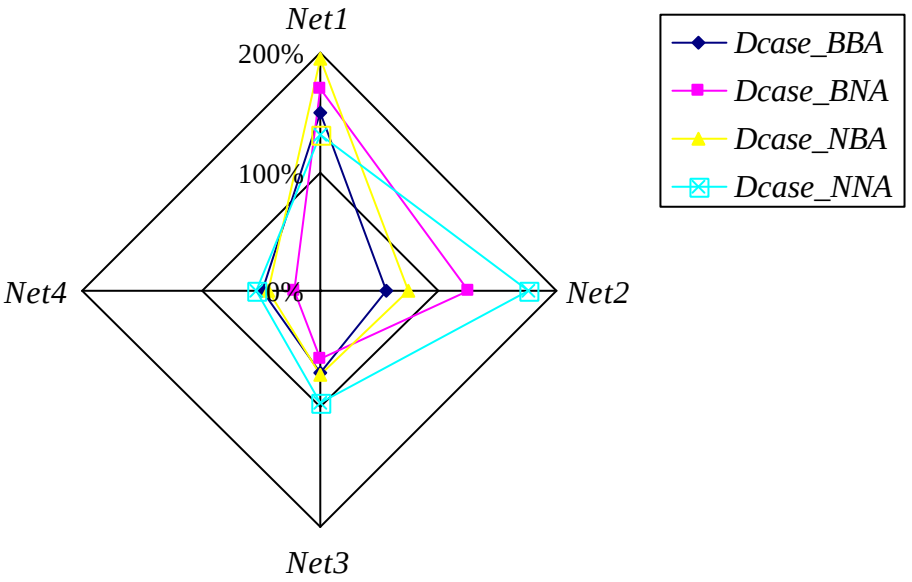

Figure 7.36 Relative increments in prediction error of each decentralized monitoring network for *Dclass_*k_1&k_2 (using acceleration measurements)

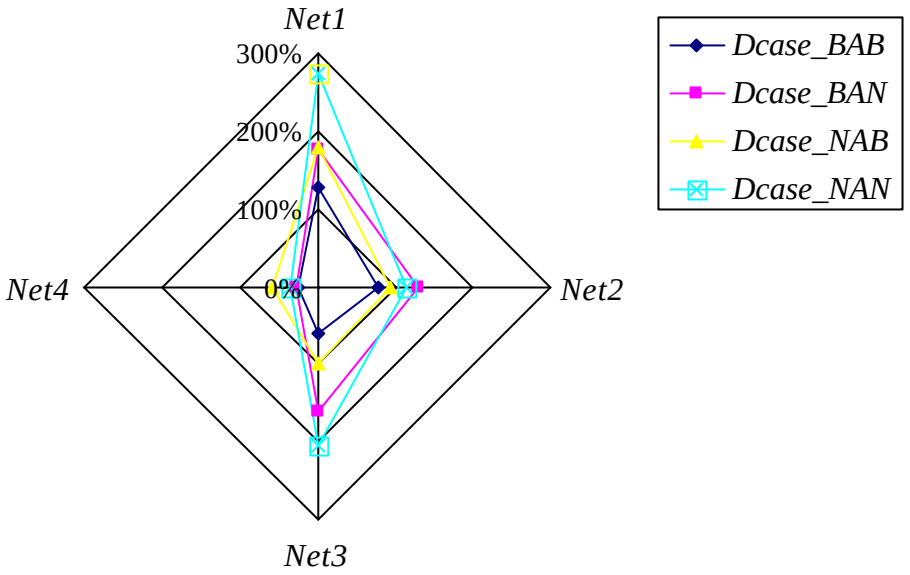

Figure 7.37 Relative increments in prediction error of each decentralized monitoring network for *Dclass_* k_1&k_3 (using acceleration measurements)

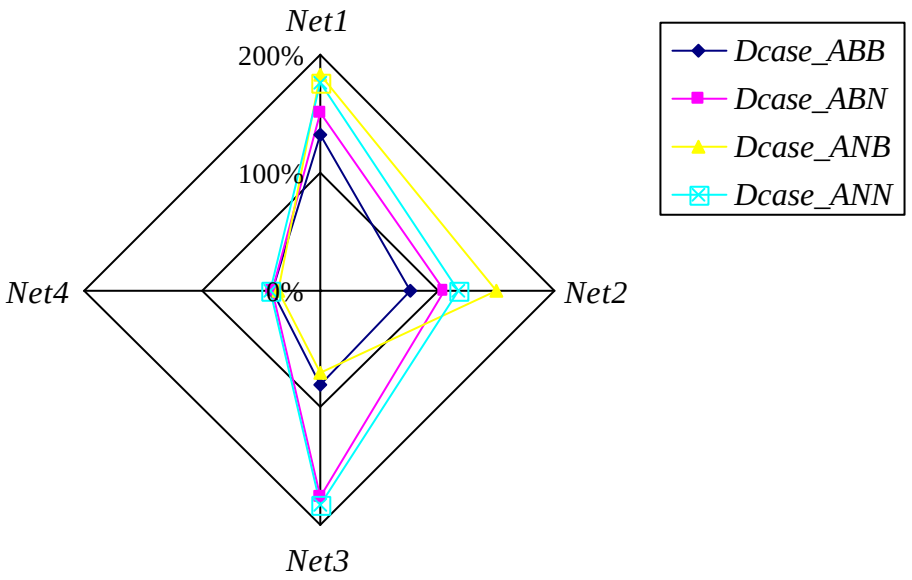

Figure 7.38 Relative increments in prediction error of each decentralized monitoring network for *Dclass_* k_2&k_3 (using acceleration measurements)

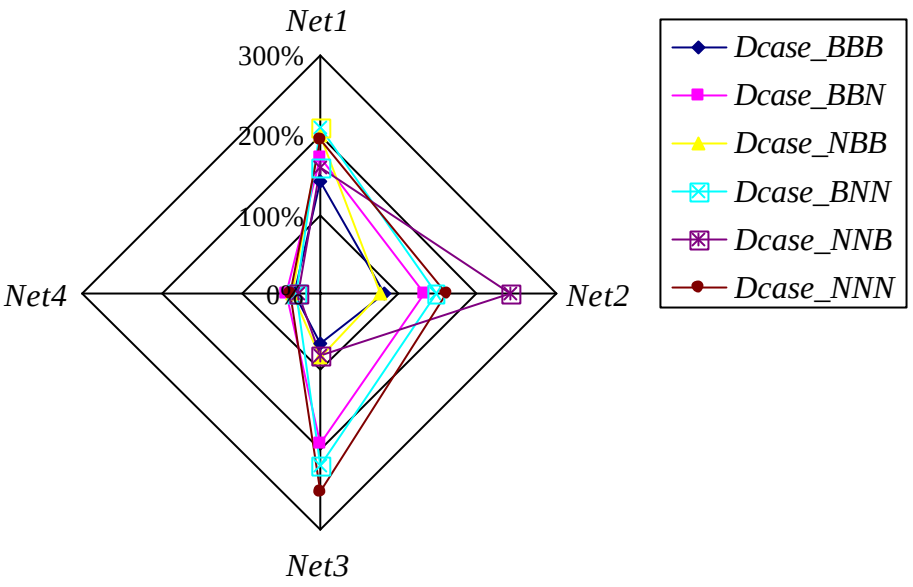

Figure 7.39 Relative increments in prediction error of each decentralized monitoring network for *Dclass_*k_1&k_2&k_3 (using acceleration measurements)

Although the theoretical basis of using decentralized monitoring networks was developed basing on the observed acceleration measurements, the concept behind the decentralized monitoring networks is also applied to the strain measurements observed from the FBG sensors to explore the behaviors of such networks. Under this situation, there are 8 decentralized monitoring networks, denoted as Net_1 to Net_8, to be trained by the corresponding data set of the intact structure. After training, they are fed with the strain measurements of the 24 deterioration cases to monitor the variations in prediction errors. In the same way, the prediction errors are plotted in the radar diagrams, which are illustrated in Figures 7.40 to 7.46, according to the deterioration classes.

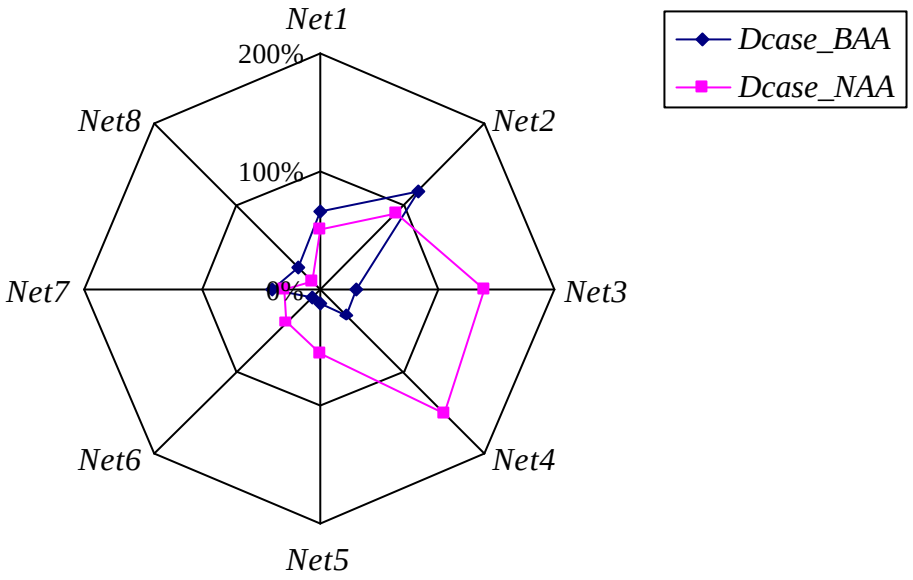

Figure 7.40 Relative increments in prediction error of each decentralized monitoring network for *Dclass*_k_1 (using strain measurements)

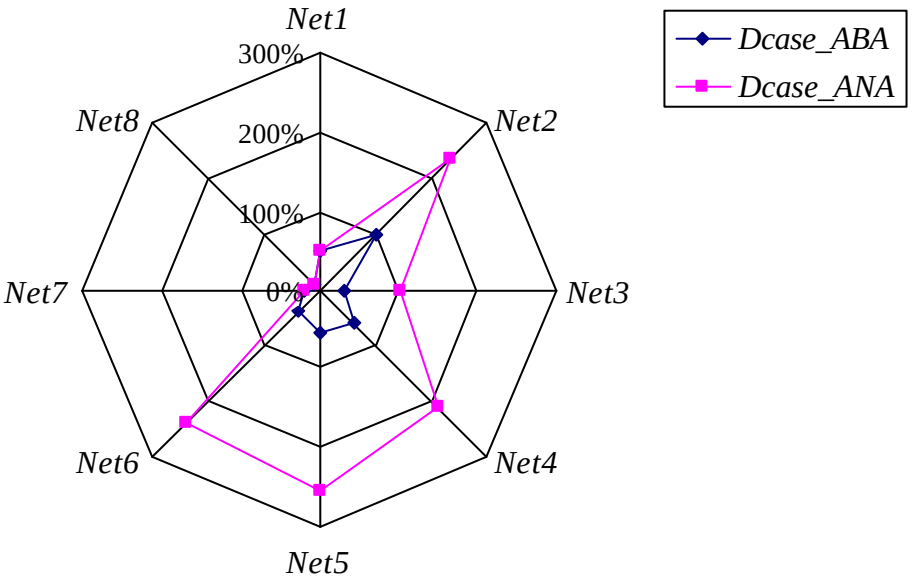

Figure 7.41 Relative increments in prediction error of each decentralized monitoring network for *Dclass*_k_2 (using strain measurements)

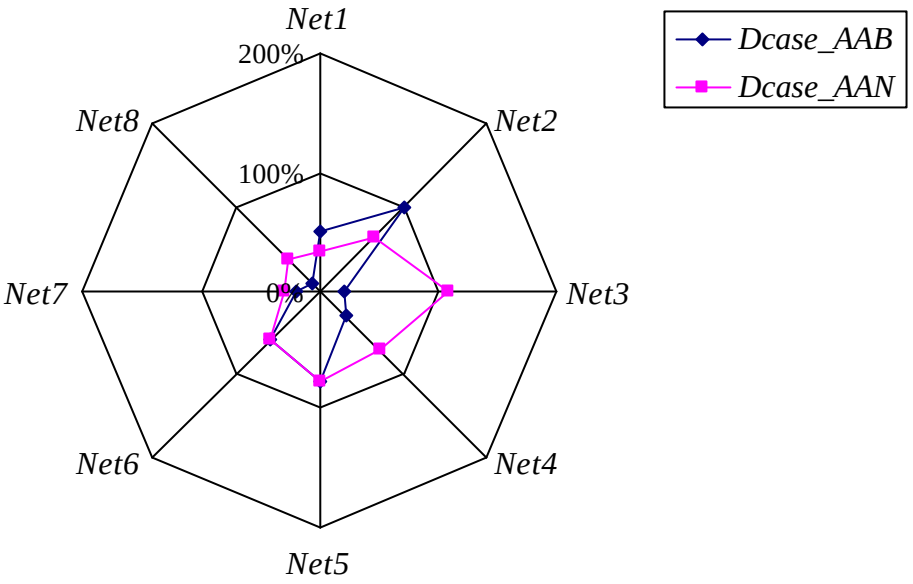

Figure 7.42 Relative increments in prediction error of each decentralized monitoring network for *Dclass_*k_3 (using strain measurements)

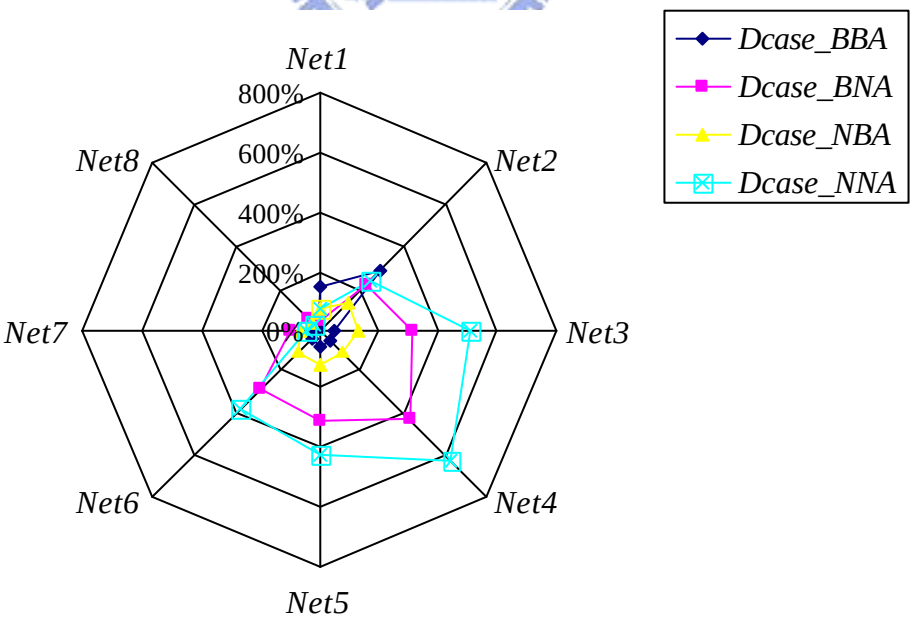

Figure 7.43 Relative increments in prediction error of each decentralized monitoring network for *Dclass_*k_1&k_2 (using strain measurements)

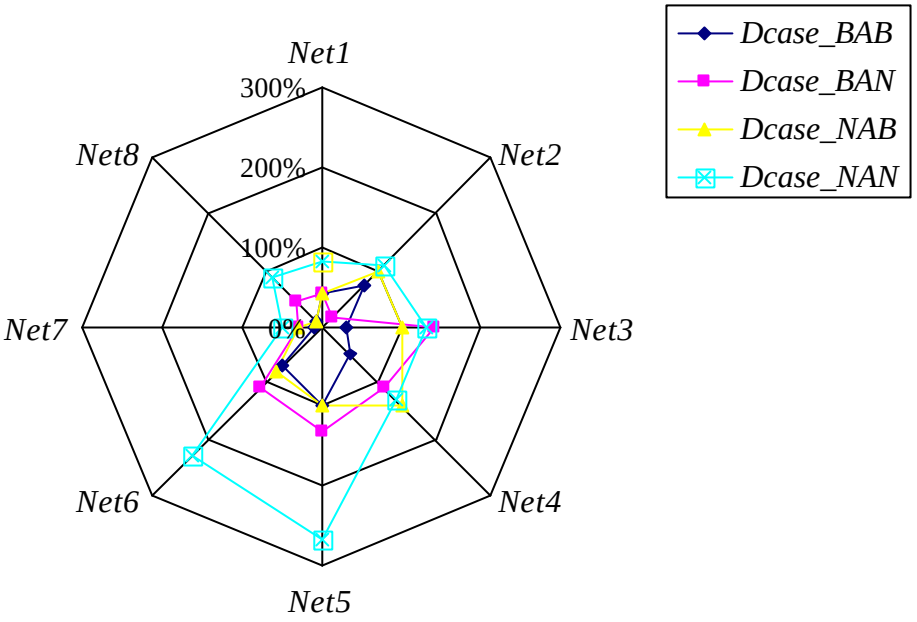

Figure 7.44 Relative increments in prediction error of each decentralized monitoring network for *Dclass_* k_1&k_3 (using strain measurements)

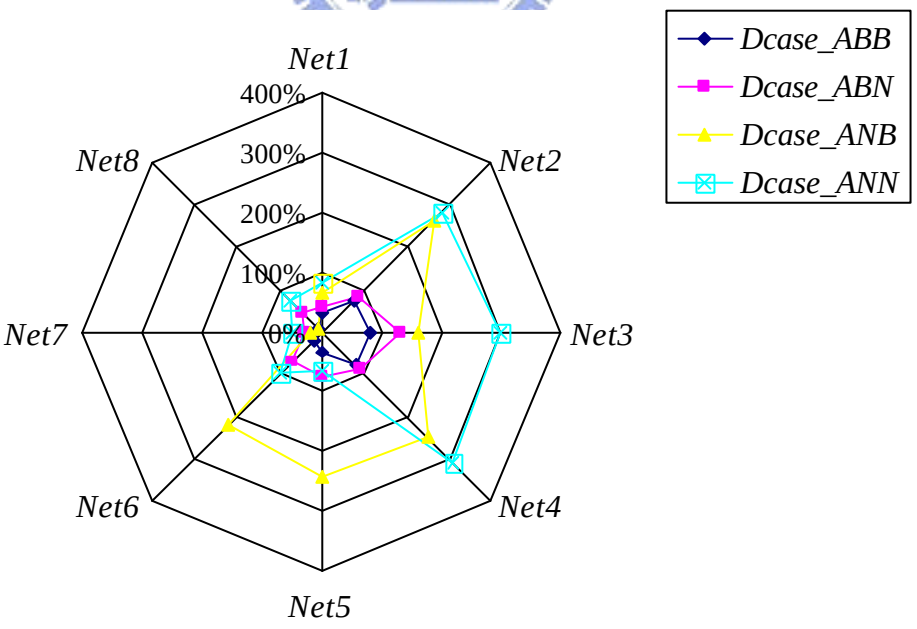

Figure 7.45 Relative increments in prediction error of each decentralized monitoring network for *Dclass_* k_2&k_3 (using strain measurements)

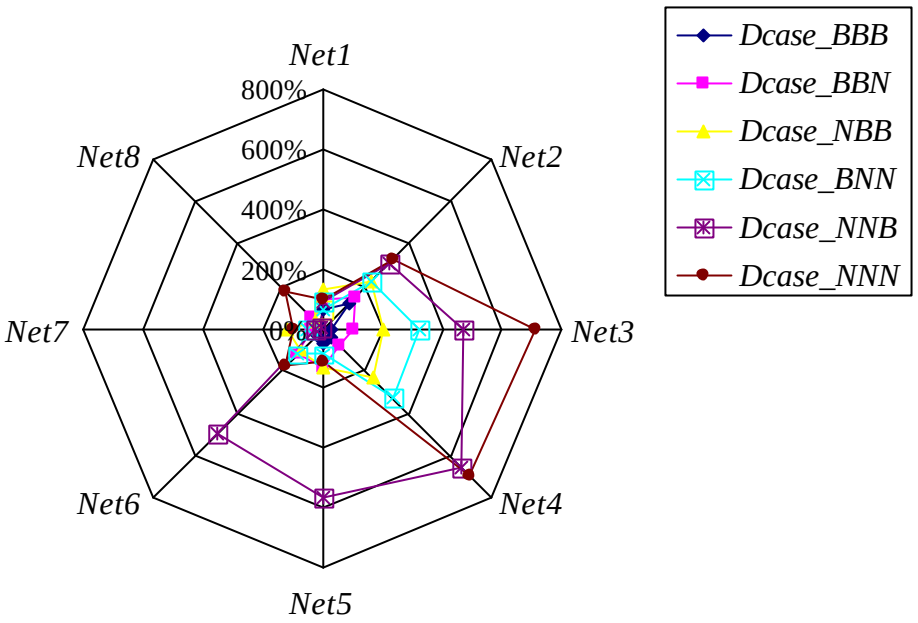

Figure 7.46 Relative increments in prediction error of each decentralized monitoring network for *Dclass*_k_1&k_2&k_3 (using strain measurements)